**Circuits and Systems**
Mekelweg 4,
2628 CD Delft
The Netherlands
http://ens.ewi.tudelft.nl/

**CAS-2019-4714881**

# M.Sc. Thesis

# Development of Data Processing Algorithms for UWB Radar-based Long-Term Health Monitoring

**Yiting Lu M.Sc.**

**Abstract**

In the last two decades, a lot of attention has been focused on contactless radar-based vital signs monitoring (heartbeat and respiration rate) as an emerging and complementary value to our medical care. It is very challenging in real indoor environments to perform concurrent localization and reliable vital signs monitoring of multiple subjects within practical distance ranges. In fact, the multipath propagation results in the reflected signal dispersed in time, which not only causes false ToF (Time of Flight) estimation but also leads to inter-subject interference, jeopardizing the vital signs extraction and the localization. Here we show a methodology based on radar techniques to automatically locate multiple subjects in indoor environments while keep monitoring their vital signs. This approach, based on the parametric models both of the propagation channel and of the radar signals, is able to cancel the undesired contributions from static clutters and multipath components, by which it is possible to accurately locate the subjects and extract their heart rates and respiration rates.

# Development of Data Processing Algorithms for UWB Radar-based Long-Term Health Monitoring

Thesis

submitted in partial fulfillment of the
requirements for the degree of

Master of Science

in

Electrical Engineering

by

Yiting Lu M.Sc.
born in Jiaxing, People's Republic of China

This work was performed in:

Circuits and Systems Group
Department of Microelectronics & Computer Engineering
Faculty of Electrical Engineering, Mathematics and Computer Science
Delft University of Technology

**Delft University of Technology**

Delft University of Technology
Department of
Microelectronics & Computer Engineering

The undersigned hereby certify that they have read and recommend to the Faculty of Electrical Engineering, Mathematics and Computer Science for acceptance a thesis entitled **"Development of Data Processing Algorithms for UWB Radar-based Long-Term Health Monitoring "** by **Yiting Lu M.Sc.** in partial fulfillment of the requirements for the degree of **Master of Science**.

Dated: 11, July, 2019

Chairman: _____
prof.dr.ir. A.J. van der Veen

Advisor: _____
dr. M. Mercuri

Committee Members: _____
prof.dr. A. Yarovoy

_____

# Abstract

In the last two decades, a lot of attention has been focused on contactless radar-based vital signs monitoring (heartbeat and respiration rate) as an emerging and complementary value to our medical care. It is very challenging in real indoor environments to perform concurrent localization and reliable vital signs monitoring of multiple subjects within practical distance ranges. In fact, the multipath propagation results in the reflected signal dispersed in time, which not only causes false ToF (Time of Flight) estimation but also leads to inter-subject interference, jeopardizing the vital signs extraction and the localization. Here we show a methodology based on radar techniques to automatically locate multiple subjects in indoor environments while keep monitoring their vital signs. This approach, based on the parametric models both of the propagation channel and of the radar signals, is able to cancel the undesired contributions from static clutters and multipath components, by which it is possible to accurately locate the subjects and extract their heart rates and respiration rates.

# Acknowledgments

First of all, I would like to thank my supervisor, Prof. van der Veen, who gave me numerous valuable advice about my master thesis. As a beginner without any practical project experience, it is his step-by-step guide that led me to the correct track. I am really appreciated about his patience and kindness during every meeting, giving me lots of insights about the algorithms and explaining everything in details. Research is tough and boring, I am very grateful for the encouragements Prof. van der Veen has given to me.

Secondly, I want to thank my daily supervisor, Dr. Mercuri, for giving me such a good opportunity to achieve my student intern at imec, the Netherlands and providing me such an interesting master thesis project. Every brain storm with Dr. Mercuri was one of the best memories at imec and I learned quite a lot from his creative and critical thinking. Thanks to his trust and the research freedom he gave to me, I could freely explore my ideas. I feel very lucky to have a supportive and friendly supervisor.

Special thanks to my friends that I met in Dalian Maritime University, Jessie Gu, Xiao Cui, Chenyu Shen and Liwei Jiang. They inspired me to study abroad and customize my own future instead of copying from others. Though we finally went to different countries and regions, the good thing is we are all clear about our future plan and will not be influenced by others, that's what really counts. Living and studying abroad is not only a journey to explore different cultures and different ways to live, but also a journey to re-discover myself. I will never regret to pursue a master degree in the Netherlands.

Huge thanks to all the sweethearts I met in TU Delft, especially Jinzi Qi, Xin Li, Xiaolin Lu, Yuhan Xu, Yaonian Cui and Shang Xiang. Thanks them for accompanying me always, whenever I felt lonely, stressed or disappointed at myself. They made Delft a second hometown for me. Every time I went back to Delft, I was surrounded with absolutely supportive and humorous friends. It was good to have someone to listen to my happiness and sufferings and to be needed when someone else was in need. Master program of course has an ending but our friendship is definitely endless.

What's more, thanks to all the intern students at Holst Centre. They helped me collect the experimental measurement which was a very important part of my thesis. Those interesting lunch talks with them were really helpful to relief the stress and anxiety from the thesis. Particular thanks to Eric and Tabea, two kindest people I've ever met in Eindhoven. Moments we shared together are unforgettable for me.

Last but not least, I want to express my massive gratitude to my parents who gave me sufficient financial support and always respected my ideas and thoughts. They fully believed in me and dedicated their selfless love to me. I know how difficult for them to allow me to study abroad because I am the only child in my family. But they still chose to support my decision just because my mother thought I would be more healthy if the air quality and food security are more guaranteed. I feel so fortunate to have such great parents.

Yiting Lu M.Sc.
Delft, The Netherlands
11, July, 2019

# Contents

# List of Figures

# List of Tables

# 1 Introduction

Radar technologies have been intensively investigated as an emerging key in health care from which not only the elderly population, caregivers, clinicians but also economy can obtain several benefits[1–9]. The primary application of interest is multi-people contactless (non-invasive) vital signs monitoring, namely the remote sensing of the heartbeat and respiration rate.

## 1.1 Problem Statement

However, the largest challenge in indoor environments is to properly locate the seated/lying down (in sofas, chairs, beds, ...) subjects and to accurately monitor their vital signs parameters. In fact, an unavoidable problem is the severe multipath effect[10–12]. In wireless communications, a reflected signal goes through a multipath channel and then arrives at the receiver. Each path has its own delay and loss, making it difficult to estimate the ToF of the direct path and leading to inter-subject interference. As a result, precise indoor localization and vital signs monitoring by non-contact radar are still calling for a robust solution. This gets more problematic in presence of static reflectors (i.e., clutters, objects). To the present, the cancellation of interference from static reflectors and the effect of the multipath effect on radar signals was not sufficiently considered and addressed.

## 1.2 Related Works

In the current state-of-the-art, pure Continuous Wave (CW) radars have been extensively used to monitor the vital signs of a single person[13–23]. Due to its narrowband nature, these architectures are not able to determine absolute distances and to separate reflections temporally. This means that it cannot monitor multiple subjects and the detection sensitivity is strongly influenced by static reflectors and multipaths.

UWB (Ultra-Wide-Band) radar architectures have been demonstrated to locate multiple persons and monitor their vital signs only under the assumption that the signals coming from different individuals do not interfere each other, meaning the subjects can be treated independently[24–31]. Based on the single target or on the independent multi-targets assumptions, in addition to the basic Doppler phase extraction[30], techniques like wavelet decomposition[16], independent component analysis (ICA)[17], complex signal demodulation[18], arctangent demodulation[19], and principal component analysis (PCA)[29] have been investigated to retrieve the vital signs parameters. Using these techniques, in most of the current state-of-the-art works, the vital signs extraction is performed after a prior knowledge of the position(s) of the subject(s),

namely the Doppler information is extracted from the range bin(s) where the person(s) is(are) present.

Some solutions have been also proposed for automatic target localization based on vital signs[13, 31]. [13] eliminates the constant reflections from static objects by performing background subtraction. The time varying information due to physiological motions can still be preserved and be regarded as the signature of identifying human targets. [31] proposed that increasing the number of Tx-Rx pairs can suppress the multipath interference. This can be realized by either using one transmitter and a large number of receivers or multiple transmit and receive antennas. The former one doesn't scale well for multiple users and the latter one causes interference between different FMCW transmitters.

In summary, the aforementioned techniques and approaches fail to deal with multi-target case in presence of multipath propagation phenomenon which generates ghost targets due to the replicas of reflected signals and fake targets caused by the combinations of reflected signals from different targets.

## 1.3 Thesis Objectives

A distinction needs to be done for both single target and the multi-target scenarios.

In the first case, with pure CW architectures, the subject and ghost targets combine together, generating an overall distorted Doppler signal while, with UWB architectures, the performance of localization is influenced by multipath components.

In case of multiple targets, and therefore UWB architectures, the multipaths caused by a subject combine with the reflected signals of other subjects and static objects, generating false Doppler signals which jeopardize the vital signs extraction and the localization.

In this work, we show a methodology, based on a Single Input Single Output (SISO) Frequency-Modulated Continuous Wave (FMCW) radar, which is able to get rid of the undesired contributions from multipath components and static reflectors. It is possible to accurately locate the subjects and extract vital signs. The proposed technique is also free of the resolution problem in Fast Fourier transform (FFT) based methods with a limited data length. In addition, we present corresponding models of the physiological motions, of the propagation channels, and of the radar signals.

In conclusion, the main objectives of this thesis project are as follows:

- Automatically locate multiple stationary subjects in a practical indoor situation using FMCW radar system with only one transceiver.
- Demodulate the physiological motions from Doppler signals.
- Estimate the vital signs of each subject, including heartbeat and respiration.

## 1.4 Thesis Structure

The thesis is organized as follows:

- Chapter 2 will introduce the radar-based long term health monitoring system, theoretical background of FMCW radar positioning and the model of physiological activities.
- Chapter 3 will derive the array signal model after considering multipath propagation channel and multiple users.
- The MUSIC (MUltiple SIgnal Classification) algorithm will be presented in Chapter 4.
- In chapter 5, the ICA (Independent Component Analysis) algorithm which is more suitable for multi-user case will be described.
- Simulation will be done in Chapter 6.
- Experimental validation and performance evaluation will be shown in Chapter 7.
- Final conclusion and future work will be given in chapter 8.

# Radar-based Health Monitoring System

# 2

The non-contact health monitoring system aims to monitor the Respiration Rate (RR) and Heartbeat Rate (HR) of multiple stationary subjects. Fig.2.1 is the sketch of the whole system which consists of an FMCW radar, two subjects and plenty of static reflectors. Due to the limitation of single transceiver, our radar system only provides 1D spatial information. The room is divided into small range cells with range resolution $\Delta d$. All the objects in the system are assumed to be point scatters. To make the subjects physically separable, different subjects are assumed to fall into different range bins but reflectors can exist anywhere.

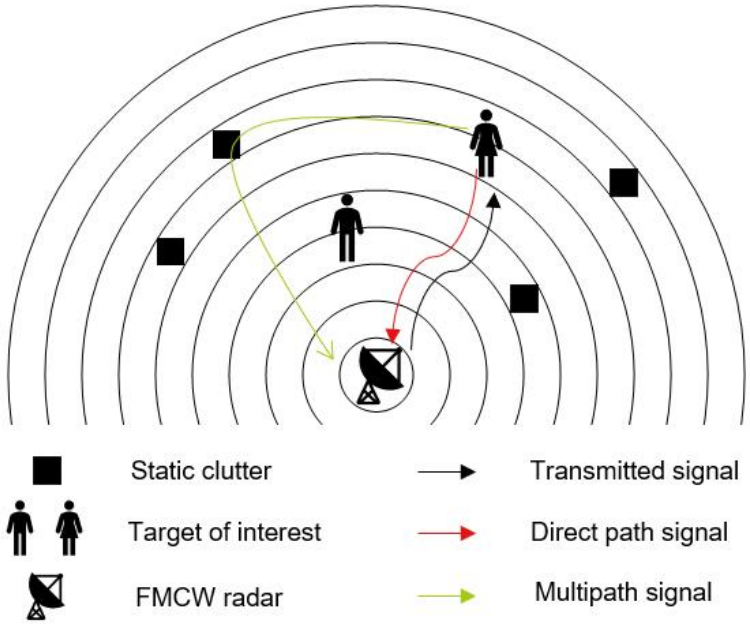


Figure 2.1: Radar system

The electromagnetic waves are sent into the environment by the transmitting antenna and are reflected by all the objects in the room, carrying the range and physiological information. Those reflected signal arrive at the receiving antenna through multiple paths, introducing different ToFs and making the indoor localization and vital sign monitoring more complicated.

## 2.1 Theoretical Background of FMCW Radar

The transmitted signal of an FMCW radar system is an up-chirp signal, also named as a sweep signal, whose frequency is linearly modulated in time, as is shown in Fig.2.2. In signal processing, the transmitted chirp signal $s_T(t)$ is usually expressed in complex form,

$$\begin{aligned} s_T(t) &= a_T e^{j2\pi \int_0^t (f_0+\rho t)dt} \\ &= a_T e^{j2\pi(f_0+\frac{\rho}{2}t)t}, 0 < t < T_c \end{aligned} \tag{2.1}$$

$a_T$ is the complex amplitude, indicating the transmitted power and the initial phase, $f_0$ is the starting frequency, the positive constant $\rho$ is the rate of frequency change, $T_c$ is the sweep period.

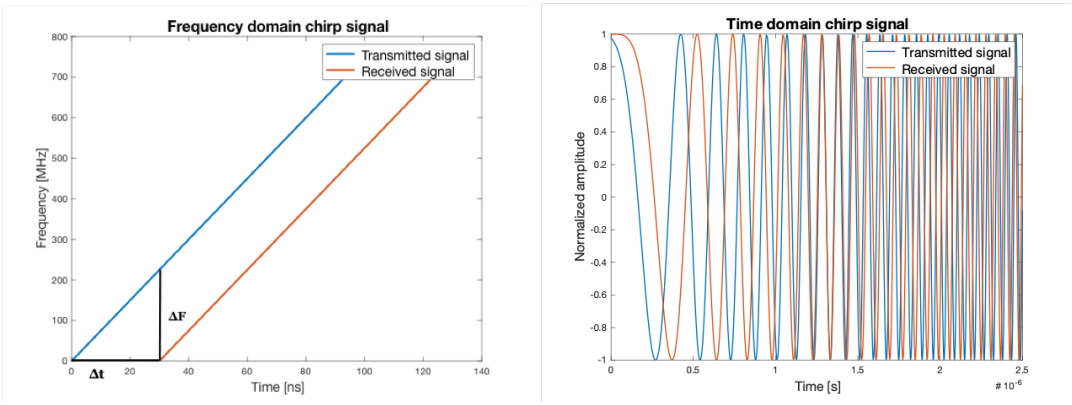


(a) frequency domain (b) time domain

Figure 2.2: Example of chirp signal

The corresponding reflected signal $s_R(t)$ is nothing but a delayed and attenuated copy of the transmitted signal,

$$\begin{aligned} s_R(t) &\propto s_T(t-\tau) \\ &= a_R e^{j2\pi\left(f_0+\frac{\rho}{2}(t-\tau)\right)(t-\tau)} \end{aligned} \tag{2.2}$$

$a_R$ is the complex amplitude of the received signal, including the energy loss and phase shift due to the reflection and path loss, $\tau$ is the two-way propagation delay of a certain path.

## 2.2 Doppler Effect

Fig.2.3 depicts block diagram of range measurement principle FMCW radar system. The shifted reflected signal mixes a copy of transmitted signal stored at the Local

Oscillator (LO), generating a beat-frequency signal $s_B(t)$,

$$\begin{aligned} s_B(t) &= a_T a_R e^{j2\pi(f_0+\frac{\rho}{2}t)t} \cdot e^{-j2\pi\left(f_0+\frac{\rho}{2}(t-\tau)\right)(t-\tau)} \\ &= a_T a_R e^{j2\pi\left(f_0\tau-\frac{\rho}{2}\tau^2+\rho\tau t\right)} \\ &\approx a_T a_R e^{j2\pi(f_0\tau+\rho\tau t)} \\ &= \underbrace{a_T a_R e^{j2\pi f_0\tau}}_{a_B} e^{j2\pi\cdot\rho\tau t} \\ &= a_B e^{j2\pi\cdot\rho\tau t}, \end{aligned} \tag{2.3}$$

here $a_B$ is the complex amplitude of the beat frequency signal and the quadratic term is neglected as it is very small. From equation (2.3), we can know that the beat-frequency signal of each reflected signal is a tone with beat frequency $f_B = \rho\tau$, which is proportional to the propagation delay $\tau$. Intuitively, from Fig.2.2a, we also can see that the frequency difference between the transmitted signal and the received signal is linearly correlated with propagation delay, if ignoring the edge effect at the start and end of the sweep.

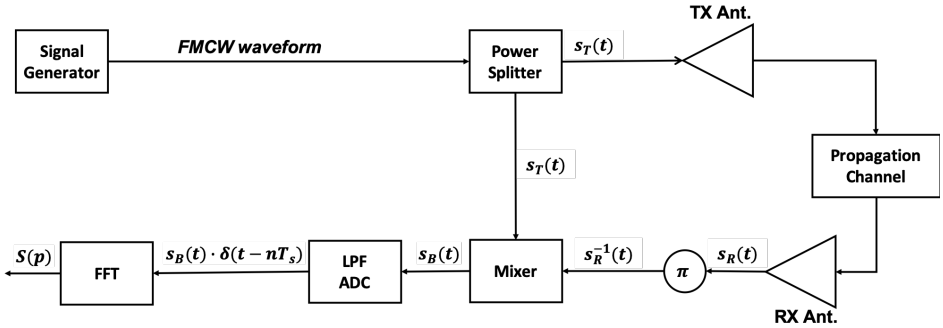


Figure 2.3: Block diagram of radio signal processing for a single chirp

Since the propagation delay is decided by the length of the propagation path

$$\tau = \frac{2d_0}{c}, \tag{2.4}$$

here $d_0$ is the path distance, $c$ is the speed of light. Once we know the beat frequency, which can be easily estimated by performing Fast Fourier Transform (FFT), we know the path distance

$$d_0 = \frac{\tau c}{2} = \frac{f_B c}{2\rho}. \tag{2.5}$$

This is the principle of range measurement in FMCW radar system.

For human subjects, the beat-frequency signal has a Doppler component because of the physiological motions which introduce some vibration in range detection. In this case, the propagation delay is not a constant but a function of time, $\tau(t)$. This small variation detected by the radar can be utilized to realize the vital signs monitoring in our system.

## 2.3 Physiological Activity Model

Non-contact health monitoring is based on remote sensing of cardiopulmonary activities, heartbeat and respiration. The inhalation and exaltation processes during breathing and the contracting and relaxing of the atria and ventricles when pumping blood through the heart all have contribution to the chest surface motion, which is a disturbance source in range detection. [32] proposed accurate statistical models for heartbeat and respiration. But the number of parameters of such precise models are too high and those parameters might not well identifiable; therefore, less sophisticated models are used in practice.

Based on the assumption that the chest surface motion is a short-term stationary process, a commonly used parametric model of heartbeat component $y_h(t)$ is a sine wave,

$$y_h(t) = a_h \cos(\omega_h t + \phi_h), \tag{2.6}$$

where $a_h$, $\omega_h$ and $\phi_h$ are deterministic, unknown amplitude, angular frequency and initial phase of the heartbeat signal [32]. Similarly, the respiration component $y_r(t)$ can also be modeled in the same way,

$$y_r(t) = a_r \cos(\omega_r t + \phi_r), \tag{2.7}$$

where $a_r$, $\omega_r$ and $\phi_r$ are deterministic, unknown amplitude, angular frequency and initial phase of the respiration signal in a short term. Therefore, the chest surface motion $y(t)$ as the sum of two sine waves,

$$\begin{aligned} y(t) &= y_h(t) + y_r(t) \\ &= a_h \cos(\omega_h t + \phi_h) + a_r \cos(\omega_r t + \phi_r). \end{aligned} \tag{2.8}$$

The amplitude of movements caused by heartbeat falls in to the range of $0.2 - 0.5$ mm and the chest surface motion due to respiration has an amplitude range of $4-12$ mm[33]. Thus the heartbeat is very weak compared with the respiration. The respiration and heartbeat frequency is usually within the range $0.1 - 0.8$ Hz and $0.8 - 2$ Hz respectively [32].

If considering this disturbance in range detection, the corresponding time-varying path distance $d(t)$ and propagation delay $\tau(t)$ are

$$d(t) = d_0 + y(t), \tag{2.9}$$

$$\tau(t) = 2\frac{d_0 + y(t)}{c}. \tag{2.10}$$

## 2.4 Range Resolution and Ambiguity

From equation 2.3, we know that the beat frequency is related to time delay and path distance which is our signal of interest. Assume $w(t) = \delta(t - nT_s)$, where $T_s$ is the

fast time sampling interval and $n$ is from 0 to $N-1$, is a window function, e.g., a rectangular window. The DTFT of the beat-frequency signal with $N$ samples is

$$\begin{aligned} S(\omega,t) &= \mathcal{F}\{s_B(t)\cdot w(t)\} \\ &= \mathcal{F}\{a_B e^{j2\pi\cdot\rho\tau(t)t}\cdot w(t)\} \\ &= |a_B| e^{\angle a_B}\delta(\omega - 2\pi\cdot\rho\tau(t)) * W(\omega) \\ &= |a_B| e^{j2\pi f_0\tau(t)} W\left(\omega - 2\pi\cdot\rho\tau(t)\right) \\ &= \underbrace{|a_B| e^{j4\pi f_0\frac{d_0}{c}} W\left(\omega - 2\pi\cdot\rho\tau(t)\right)}_{A(\omega)} \underbrace{e^{j4\pi f_0\frac{y(t)}{c}}}_{e^{j\phi(t)}} \\ &= A(\omega)e^{j\phi(t)} \end{aligned} \tag{2.11}$$

where $\mathcal{F}\{\cdot\}$ is the DTFT operation, $\delta\{\cdot\}$ is the impulse function and $W(\omega)$ can be a sinc function, $\frac{\sin(N\omega/2)}{\sin(\omega/2)}e^{-j\omega N/2}$. In practice, $S(\omega,t)$ is estimated via an FFT whose result is denoted as $S(k,t)$, which is a sampled version of DTFT,

$$\begin{aligned} S(k,t) &= A(\omega)e^{j\phi(t)}\cdot\delta(\omega - \frac{2\pi k}{N}) \\ &= \underbrace{A(\omega)\delta(\omega - \frac{2\pi k}{N})}_{A(k)} e^{j\phi(t)} \\ &= A(k)e^{j\phi(t)} \end{aligned} \tag{2.12}$$

where $k$ is the frequency bin index of FFT, from 0 to $N-1$.

As is mentioned in section 2.2, the disturbance caused by cardiopulmonary activities in range detection is regarded as the vital signs of subjects. And the range is estimated by resolving the beat frequency. However, the resolution of FFT, $\Delta f$, is restricted by the sweep period,

$$\Delta f = \frac{1}{T_c}. \tag{2.13}$$

Therefore, the range resolution $\Delta d$ of a radar system is also limited,

$$\Delta d = \frac{\Delta f c}{2\rho} = \frac{\frac{1}{T_c}c}{2\frac{B_W}{T_c}} = \frac{c}{2B_W} \tag{2.14}$$

$B_W$ is the radar bandwidth. In our system, $B_W = 150MHz$, thus $\Delta d = 0.2m$. The amplitude of chest surface motion in section 2.3 is around $1cm$, so the frequency resolution is not sufficient to reflect the chest surface motion. However, the phase of the resulting frequency domain signal $S(\omega,t)$ still preserves the Doppler information.

For a fixed $k$, $S(k,t)$ is a complex signal with a magnitude, $|A(k)|$, a constant phase component, $\angle A(k)$, and a time varying phase, $\phi(t)$, resulting an arc in the complex plane. Therefore, our signal of interest is then the phase of $S(k,t)$, which is proportional to the chest surface motion, calling for phase demodulation steps to estimate the vital signs.

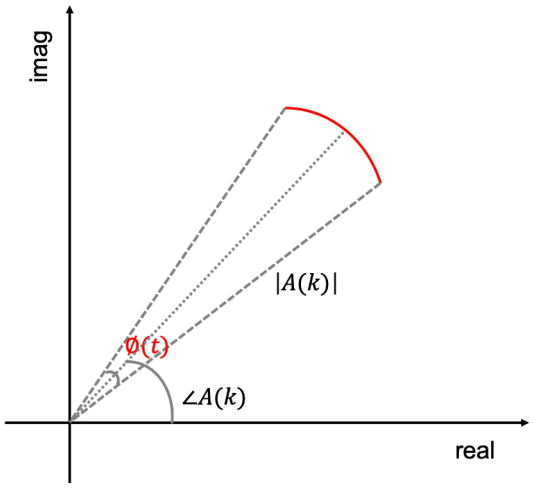


Figure 2.4: Complex plane visualization of $S(k,t)$

# 3 Array Signal Model

Array signal processing methods are widely used in statistical signal processing domain. Observation signal is extended from a 1D vector to high dimensional matrix, bringing novel solutions for problems such as determining the number and locations of sources, enhancing the Signal-to-Interference-plus-Noise Ratio (SINR), tracking moving objects and Blind Source Separation (BSS). The main tasks of this project are automatic people tracking & counting and source separation, both of them are well-suited for array signal processing.

## 3.1 FMCW Matrix

Fig.3.1 shows that, in practice, chirps are sent one after one and the corresponding received chirps are stacked in columns, forming an FMCW matrix for future processing. The resulting matrix has two dimensions, fast-time and slow-time, both are discrete in reality.

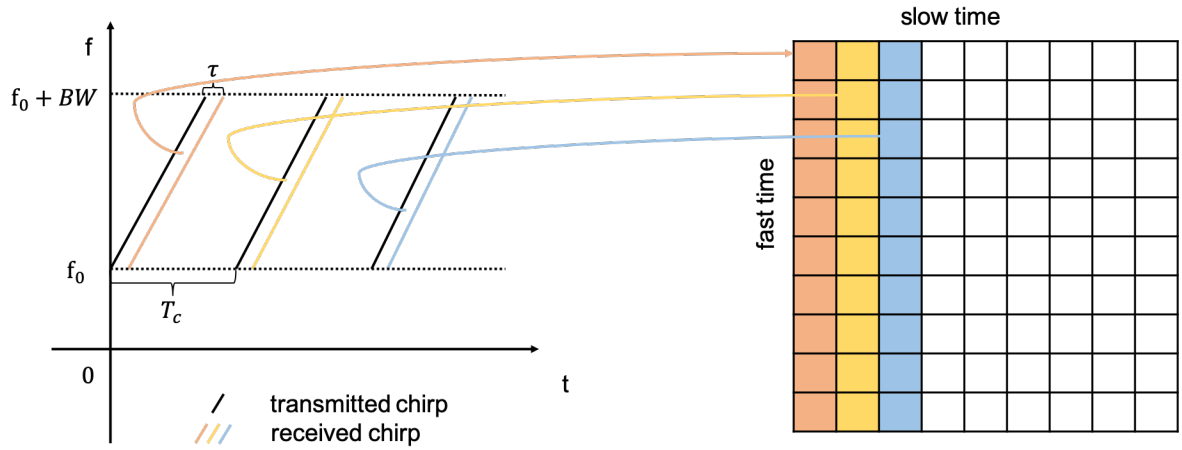


Figure 3.1: FMCW matrix

The basic idea of doing signal processing for FMCW matrix consisting of two steps, processing along fast-time column by column to obtain the range profile and processing along slow-time row by row to extracting vital sign information. The former one is done by FFT as is shown in Fig.3.2. Based on section 2.4, each column in the resulting matrix gives us a spectrum. Assume the slow-time sampling interval is $T_s'$, the discretized

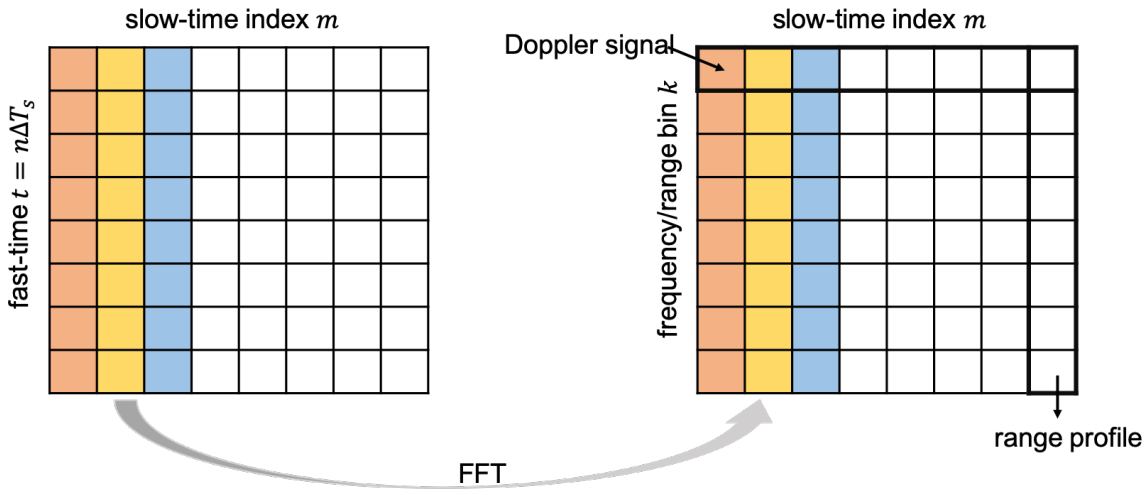


Figure 3.2: FFT of FMCW matrix

version of $S(k,t)$ is

$$\begin{aligned} S(k,m) &= A(k)\underbrace{e^{j\phi(t)}\delta(t-mT_s')}_{e^{j\phi(m)}} \\ &= A(k)e^{j\phi(m)} \end{aligned} \tag{3.1}$$

where $m$ is from 0 to $M-1$. The expression of each column degrades from equation 2.11 to a one-variable function of $k$, namely the *range profile*. Similarly, the row expression is also a one-variable function regarding to slow-time, namely the *Doppler signal*.

## 3.2 Multipath Propagation Model

In a wireless communication system, multipath interference is always an annoying issue. It occurs when a signal takes two or more paths from the transmitting antenna to the receiving antenna, resulting in ghost subjects and inter-subject interference. To address this problem, [34] proposed an accurate parametric model for indoor multipath propagation, widely known as Saleh-Valenzuela Model. It states that in an indoor environment, the reflected rays arrive at the receiving antenna in clusters. The power gain of different clusters and of rays within a cluster obey the exponential power decay.

The statistical properties of Saleh-Valenzuela Model is difficult to make use. In [35], Jakes popularized a less sophisticated and less parametric channel which still keeps the essential properties of the physical propagation model.

Based on the limited room size, we only consider the first $L$ frequency components; therefore, the number of reflected paths is also $L$. It comes with the assumption that the multipath propagation channel $h(t)$ is an Finite-length Impulse Response (FIR) filter of at most $L$ symbols. This channel is represented by multiple paths having complex power gain $\{\beta_l\}$ and propagation delay $\{\tau_l\}$, where $l$ is the path index, the resulting

channel impulse response is as follows,

$$h(t) = \sum_{l=0}^{L-1} \beta_l \delta(t - \tau_l). \tag{3.2}$$

It is a generalization of all the possible propagation models that occur in practice. Though it is not a structured one, we can still specify the statistical properties of the model coefficients at a later stage. Therefore, the received parametric signal model $s_R(t)$ over a multipath channel can be corrected as the convolution

$$\begin{aligned} s_R(t) &= h(t) * s_T(t) \\ &= \left[ \sum_{l=0}^{L-1} \beta_l \delta\left(t - \tau_l(t)\right) \right] * s_T(t) \\ &= \sum_{l=0}^{L-1} \beta_l s_T\left(t - \tau_l(t)\right) \\ &= \sum_{l=0}^{L-1} \underbrace{\beta_l a_{T_l}}_{a_{R_l}} e^{j2\pi\left(f_0 + \frac{\rho}{2}(t-\pi_l(t))\right)(t-\tau_l(t))} \\ &= \sum_{l=0}^{L-1} a_{R_l} e^{j2\pi\left(f_0 + \frac{\rho}{2}(t-\pi_l(t))\right)(t-\tau_l(t))}. \end{aligned} \tag{3.3}$$

The corresponding baseband signal model $s_B(t)$ is then

$$\begin{aligned} s_B(t) &= \sum_{l=0}^{L-1} s_R(t) \cdot s_T^{-1}(t) \\ &= \sum_{l=0}^{L-1} \underbrace{a_T a_R e^{j2\pi f_0 \tau_l(t)}}_{a_{B_l}(t)} e^{j2\pi \cdot \rho \tau_l(t) t} \\ &= \sum_{l=0}^{L-1} a_{B_l}(t) e^{j2\pi \cdot \rho \tau_l(t) t} \\ &= \sum_{l=0}^{L-1} s_{B_l}(t). \end{aligned} \tag{3.4}$$

After performing FFT in fast-time, the frequency domain signal $S(k,m)$ becomes

$$\begin{aligned} S(k,m) &= \mathcal{F}\left\{\sum_{l=0}^{L-1} s_{B_l}(t)\cdot w(t)\right\}\cdot\delta(t-mT_s') \\ &= \sum_{l=0}^{L-1}\mathcal{F}\left\{s_{B_l}(t)\cdot w(t)\right\}\cdot\delta(t-mT_s') \\ &= \underbrace{\sum_{l=0}^{L-1} A_l(k)\, e^{j\phi(m)}}_{A'(k)} \\ &= A'(k)e^{j\phi(m)}. \end{aligned} \tag{3.5}$$

## 3.3 Matrix Factorization

The aforementioned observation signal $S(k,m)$ in equation 3.5 is a dual-variable function of frequency index $k$ and discrete slow-time $m$, forming a 2D observation matrix denoted as $\mathbf{X}$. To explore the characteristics of the observation matrix, it is necessary to do matrix factorization to isolate the signal of interest. Then the observation matrix $\mathbf{X}$ including all the samples becomes

$$\begin{aligned} \mathbf{X} &= \begin{bmatrix}\mathbf{x}_0 & \mathbf{x}_1 & \cdots & \mathbf{x}_{M-1}\end{bmatrix} \\ &= \begin{bmatrix} S(0,0) & S(0,1) & \cdots & S(0,M-1) \\ S(1,0) & S(1,1) & \cdots & S(1,M-1) \\ \vdots & \vdots & \ddots & \vdots \\ S(L-1,0) & S(L-1,1) & \cdots & S(L-1,M-1)\end{bmatrix} : L\times M. \end{aligned} \tag{3.6}$$

It follows that $\mathbf{X}$ has a factorization

$$\mathbf{X} = \mathbf{hs} \tag{3.7}$$

where

$$\mathbf{s} = \begin{bmatrix}e^{j\phi(0)} & e^{j\phi(1)}\cdots & e^{j\phi(M-1)}\end{bmatrix} : 1\times M, \quad \mathbf{h} = \begin{bmatrix} A'(0) \\ A'(1) \\ \vdots \\ A'(L-1)\end{bmatrix} : L\times 1, \tag{3.8}$$

Here $\mathbf{s}$ contains the Doppler information due to the physiological activities. Time shifts in propagation delay resulting in frequency/range shifts in range profile; therefore $\mathbf{h}$ contains the attenuation and time delay information of the propagation channel for each reflector. Obviously, $\mathbf{X}$ is a rank-1 matrix and it spans the same row space with $\mathbf{s}$. However, this is the data model for single user case, in a real indoor environment, there are a lot of static clutters and what we are interested in is the multi-user case. So this simple model is going to be extended to a more complicated one for more practical applications.

## 3.4 Extension to Multi-User Case

Assume that there are $P$ subjects and $Q$ static clutters in the room, all of them are regarded as point scatters. The only difference between human targets and static clutters is that human targets have physiological activities leading to a small disturbance in range detection. Therefore, for static clutters, the time delay $\tau$ is a constant, resulting in a constant phase after performing FFT. Generally, the received signal model in equation 3.3 then can be rewritten as

$$\begin{aligned} s_R(t) &= \sum_{i=1}^{P} h_i(t) * s_T(t) + \sum_{i=P+1}^{P+Q} h_i(t) * s_T(t) \\ &= \sum_{i=1}^{P} \sum_{l=0}^{L-1} \beta_{i,l} s_T(t - \tau_{i,l}(t)) + \sum_{i=P+1}^{P+Q} \sum_{l=0}^{L-1} \beta_{i,l} s_T(t - \tau_{i,l}). \end{aligned} \tag{3.9}$$

A sketch for this data model is shown in Fig.3.3. The baseband model results from

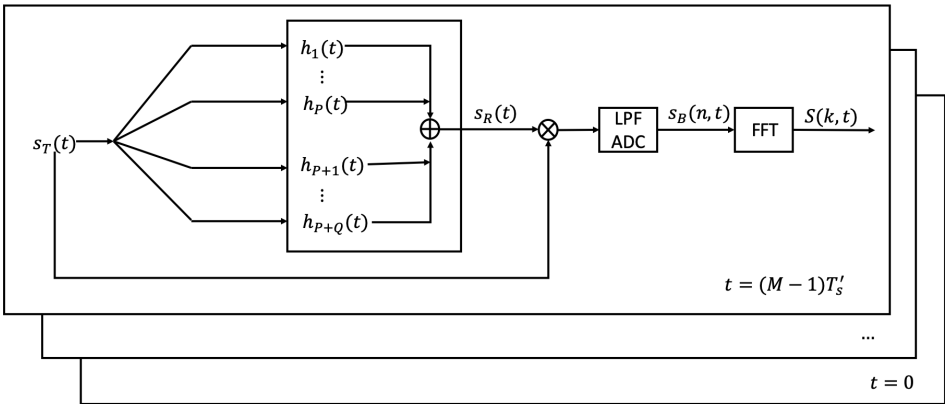


Figure 3.3: Multi-user channel model

multiple subjects and static clutters can be derived from equation 3.4 as

$$s_B(t) = \sum_{i=1}^{P} \sum_{l=0}^{L-1} a_{B_{i,l}}(t) e^{j2\pi \cdot \rho \tau_{i,l}(t) t} + \sum_{i=P+1}^{P+Q} \sum_{l=0}^{L-1} a_{B_{i,l}}(t) e^{j2\pi \cdot \rho \tau_{i,l} t}. \tag{3.10}$$

As FFT is a linear operator, the Fourier transform of a sum of functions is the sum of individual Fourier transforms, the corresponding frequency domain signl $S(p,t)$ in equation 3.5 should be rewritten as

$$S(k,m) = \sum_{i=1}^{P} A_i'(k) e^{j\phi_i(m)} + \sum_{i=P+1}^{P+Q} \underbrace{A_i'(k) e^{j\phi_i}}_{A_i'(k)} \tag{3.11}$$

where $\phi_i$ $(i = P+1, \cdots, P+Q)$ is a constant phase component thus can be concluded in the complex constant $A_i'(k)$ $(i = P+1, \cdots, P+Q)$. $\mathbf{X}$ has the following factorization

$$\mathbf{X} = \mathbf{HS} \tag{3.12}$$

where

$$\begin{aligned}\mathbf{H} &= \left[\begin{array}{ccc|ccc} A'_1(0) & \cdots & A'_P(0) & A'_{P+1}(0) & \cdots & A'_{P+Q}(0) \\ A'_1(1) & \cdots & A'_P(1) & A'_{P+1}(1) & \cdots & A'_{P+Q}(1) \\ \vdots & \ddots & \vdots & \vdots & \ddots & \vdots \\ A'_1(L-1) & \cdots & A'_P(L-1) & A'_{P+1}(L-1) & \cdots & A'_{P+Q}(L-1) \end{array}\right] \\ &= \left[\begin{array}{c|c} \mathbf{H}_P & \mathbf{H}_Q \end{array}\right] : L \times (P+Q),\end{aligned} \tag{3.13}$$

$$\begin{aligned}\mathbf{S} &= \left[\begin{array}{cccc} e^{j\phi_1(0)} & e^{j\phi_1(1)} & \cdots & e^{j\phi_1(M-1)} \\ \vdots & \vdots & \ddots & \vdots \\ e^{j\phi_P(0)} & e^{j\phi_P(1)} & \cdots & e^{j\phi_P(M-1)} \\ \hline \mathbf{1}_Q & \mathbf{1}_Q & \cdots & \mathbf{1}_Q \end{array}\right] \\ &= \left[\begin{array}{c} \mathbf{S}_P \\ \hline \mathbf{S}_Q \end{array}\right] : (P+Q) \times M\end{aligned} \tag{3.14}$$

where $\mathbf{1}_Q$ is length-$Q$ all-one vector. To isolate the contribution from subjects and static clutters, the factorization can be rewritten as

$$\begin{aligned}\mathbf{X} &= \left[\begin{array}{c|c} \mathbf{H}_P & \mathbf{H}_Q \end{array}\right] \left[\begin{array}{c} \mathbf{S}_P \\ \hline \mathbf{S}_Q \end{array}\right] \\ &= \mathbf{H}_P\mathbf{S}_P + \mathbf{H}_Q\mathbf{S}_Q\end{aligned} \tag{3.15}$$

where the second term contributes DC information in slow-time. As we actually only focus on the time varying Doppler signals from subjects, we can remove the constant sources in $\mathbf{S}$ matrix, then the data model becomes

$$\mathbf{X} = \mathbf{H}\mathbf{S} + \mathbf{C} \tag{3.16}$$

where $\mathbf{C} = \mathbf{H}_Q\mathbf{S}_Q$ is an $L \times M$ matrix with identical columns,

$$\mathbf{H} = \begin{bmatrix} A'_1(0) & \cdots & A'_P(0) \\ A'_1(1) & \cdots & A'_P(1) \\ \vdots & \ddots & \vdots \\ A'_1(L-1) & \cdots & A'_P(L-1) \end{bmatrix} : L \times P, \tag{3.17}$$

$$\begin{aligned}\mathbf{S} &= \begin{bmatrix} \mathbf{s}_0 & \mathbf{s}_1 & \cdots & \mathbf{s}_{M-1} \end{bmatrix} \\ &= \begin{bmatrix} e^{j\phi_1(0)} & e^{j\phi_1(1)} & \cdots & e^{j\phi_1(M-1)} \\ \vdots & \vdots & \ddots & \vdots \\ e^{j\phi_P(0)} & e^{j\phi_P(1)} & \cdots & e^{j\phi_P(M-1)} \end{bmatrix} : P \times M.\end{aligned} \tag{3.18}$$

In presence of additive noise, the data model can be

$$\mathbf{x}_m = \mathbf{H}\mathbf{s}_m + \mathbf{c} + \mathbf{n}_m \Leftrightarrow \mathbf{X} = \mathbf{H}\mathbf{S} + \mathbf{C} + \mathbf{N}, \tag{3.19}$$

here $m$ is from 0 to $M-1$, $\mathbf{c}$ is a column in $\mathbf{C}$. The model assumptions are summarized as follows,

- $L \leq P$.
- $\mathbf{S}$ has full row rank $P$.
- Each row of $\mathbf{S}$ is regarded as a signal from an independent source. All the signals are assumed to be random, independent, identically distributed (i.i.d.), with modulus equal to 1.
- The noise is assumed to be additive, white, zero mean, complex Gaussian distributed, with covariance $\mathbf{R}_n = E\{\mathbf{n}\mathbf{n}^H\} = \sigma^2\mathbf{I}$ and independent from the sources.
- $\mathbf{C}$ is a complex matrix with identical columns; therefore, the rank of $\mathbf{C}$ is 1.

# 4 The MUSIC Algorithm

MUltiple SIgnal Classification (MUSIC) algorithm is a widely used method for parameter estimation. Our parameters of interest here is the frequencies of heartbeat and respiration. From chapter 3, we know exactly the data model and the signal structures; therefore, in this chapter, a detailed explanation about using MUSIC to estimate parameters of interest will be introduced. To arrive at the common data model we use in statistical signal processing, a preprocessing step to remove the DC components should be done first.

## 4.1 DC Removal

Recall the array data model in equation 3.19, there is a DC term, $\mathbf{C}$, caused by the static clutters. Based on the matrix property, i.e., the columns of $\mathbf{C}$ are identical, it can be removed by doing matrix projection

$$\begin{aligned} \mathbf{XP_r} &= \mathbf{HSP_r} + \mathbf{CP_r} + \mathbf{NP_r} \\ &= \mathbf{HSP_r} + \mathbf{NP_r}, \end{aligned} \tag{4.1}$$

One possible solution of projection matrix $\mathbf{P_r}$ is

$$\mathbf{P_r} = \mathbf{I} - \frac{\mathbf{1}_M \mathbf{1}_M^T}{M}, \tag{4.2}$$

with which

$$\begin{aligned} \mathbf{CP_r} &= \mathbf{H}_Q \mathbf{1}_Q \mathbf{1}_M^T \cdot \left( \mathbf{I} - \frac{\mathbf{1}_M \mathbf{1}_M^T}{M} \right) \\ &= \mathbf{H}_Q \cdot \left( \mathbf{1}_Q \mathbf{1}_M^T - \mathbf{1}_Q \mathbf{1}_M^T \right) \\ &= \mathbf{0}. \end{aligned} \tag{4.3}$$

However, in this way, we also change the structure of $\mathbf{S}$, that is to say, the DC components in $\mathbf{S}$ are also removed after multiplying with $\mathbf{P_r}$. The influence of such undesired DC removal for the Doppler signal is shown in Fig.4.1.

Despite the rows in $\mathbf{S}$ being zero mean slow-time series, the physiological motion is still preserved. Since direct angle extraction gives us incorrect phase information, wiser ways to do phase demodulation will be covered in later chapters. Let us denote the zero mean observation matrix as $\overline{\mathbf{X}} = \mathbf{XP_r}$, zero mean signal matrix as $\overline{\mathbf{S}} = \mathbf{SP_r}$. The noise matrix is still the same, $\mathbf{N} = \mathbf{NP_r}$, because noise is assumed to be zero mean. Then the new data model becomes

$$\overline{\mathbf{X}} = \mathbf{H}\overline{\mathbf{S}} + \mathbf{N}. \tag{4.4}$$

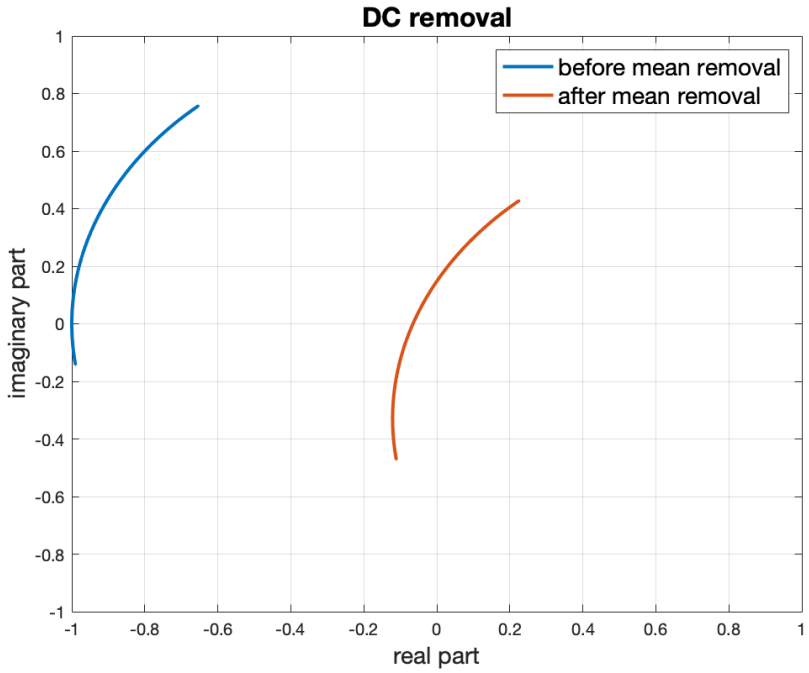


Figure 4.1: DC removal of Doppler signal

## 4.2 Approximate Data Model

Recall the source signal model in equation 3.18 which can be rewritten as

$$\mathbf{S} = \begin{bmatrix} e^{j\phi_1(0)} & e^{j\phi_1(1)} & \cdots & e^{j\phi_1(M-1)} \\ \vdots & \vdots & \ddots & \vdots \\ e^{j\phi_P(0)} & e^{j\phi_P(1)} & \cdots & e^{j\phi_P(M-1)} \end{bmatrix} = \begin{bmatrix} \mathbf{s}_1^{\mathrm{H}} \\ \mathbf{s}_2^{\mathrm{H}} \\ \vdots \\ \mathbf{s}_P^{\mathrm{H}} \end{bmatrix} \tag{4.5}$$

where each vector $\mathbf{s}_i$ ($i$ is from 1 to $P$) is a function of discrete time $m$, $s_i(m)$, $m = 0, 1, \cdots, (M-1)$. The complex Taylor expansion of $s_i(m)$ is

$$\begin{aligned} s_i(m) &= e^{j\phi_i(m)} \\ &= 1 + j\phi_i(m) - \frac{\phi_i^2(m)}{2!} + \cdots \\ &= 1 + j\frac{4\pi f_0}{c} y_i(mT_s') - \left(\frac{4\pi f_0}{c}\right)^2 \frac{y_i^2(mT_s')}{2} + \cdots \end{aligned} \tag{4.6}$$

where $y_i(mT_s')$ is physiological activity of subject $i$. Substituting $y_i(mT_s') = a_{h,i}\cos(\omega_{h,i}mT_s' + \phi_{h,i}) + a_{r,i}\cos(\omega_{r,i}mT_s' + \phi_{r,i})$ into equation 4.6,

$$\begin{aligned} s_i(m) &= j\frac{4\pi f_0}{c}\left[a_{h,i}\cos(\omega_{h,i}mT_s' + \phi_{h,i}) + a_{r,i}\cos(\omega_{r,i}mT_s' + \phi_{r,i})\right] \\ &+ \frac{1}{4}\left(\frac{4\pi f_0}{c}\right)^2\left[a_{h,i}^2\cos\left(2\omega_{h,i}mT_s' + 2\phi_{h,i}\right) + a_{r,i}^2\cos\left(2\omega_{r,i}mT_s' + 2\phi_{r,i}\right)\right] \\ &+ \frac{1}{2}\left(\frac{4\pi f_0}{c}\right)^2 a_{h,i}a_{r,i}\cos\left((\omega_{h,i} + \omega_{r,i})mT_s' + \phi_{h,i} + \phi_{r,i}\right) \\ &+ \frac{1}{2}\left(\frac{4\pi f_0}{c}\right)^2 a_{h,i}a_{r,i}\cos\left((\omega_{h,i} - \omega_{r,i})mT_s' + \phi_{h,i} - \phi_{r,i}\right) \\ &+ 1 - \frac{1}{4}\left(\frac{4\pi f_0}{c}\right)^2\left(a_{h,i}^2 + a_{r,i}^2\right) + \cdots; \end{aligned} \tag{4.7}$$

therefore, the Doppler signal is consist of a DC component and a group of harmonics. In our case, $f_0 = 7.3$ GHz, therefore, $\frac{4\pi f_0}{c}a_{r,i} \approx 1$ and $\frac{4\pi f_0}{c}a_{h,i} \approx 0.1$, an approximate model for $\bar{s}_i(m)$ can be

$$\begin{aligned} \bar{s}_i(m) &\approx \underbrace{j\frac{4\pi f_0}{c}a_{r,i}\cos(\omega_{r,i}mT_s' + \phi_{r,i})}_{\bar{s}_{i,1}(m)} + \underbrace{\frac{1}{4}\left(\frac{4\pi f_0}{c}\right)^2 a_{r,i}^2\cos\left(2\omega_{r,i}mT_s' + 2\phi_{r,i}\right)}_{\bar{s}_{i,2}(m)} \\ &= \bar{s}_{i,1}(m) + \bar{s}_{i,2}(m) \end{aligned} \tag{4.8}$$

where $\bar{s}_{i,1}(m)$ is the first harmonic which is the most powerful component and $\bar{s}_{i,2}(m)$ is the second harmonic which is the least powerful one. Thus $\overline{\mathbf{S}}$ in equation 4.4 is

$$\overline{\mathbf{S}} = \begin{bmatrix} \overline{\mathbf{s}}_1^{\mathrm{H}} \\ \overline{\mathbf{s}}_2^{\mathrm{H}} \\ \vdots \\ \overline{\mathbf{s}}_P^{\mathrm{H}} \end{bmatrix} \tag{4.9}$$

where $\overline{\mathbf{s}}_i^{\mathrm{H}} = [\bar{s}_i(0), \bar{s}_i(1), \cdots, \bar{s}_i(M-1)]$.

## 4.3 Dimension Reduction and Hilbert Transform

From equation 4.8, we know that though $\bar{s}_i(m)$ is a complex signal, it can not be written as the sum of two complex sine waves, which is the required data structure for almost all parametric methods. Assume $\overline{\mathbf{x}}_k$ and $\mathbf{h}_k$ are row vectors in $\overline{\mathbf{X}}$ and $\mathbf{H}$ respectively, $k$ is from 0 to $L-1$. There is a linear transform between $\overline{\mathbf{x}}_k$ and $\overline{\mathbf{S}}$,

$$\overline{\mathbf{x}}_k = \mathbf{h}_k\overline{\mathbf{S}}. \tag{4.10}$$

Since $\overline{\mathbf{x}}_k$ is the linear combination of rows in $\overline{\mathbf{S}}$, the data structure of $\overline{\mathbf{x}}_k$ also doesn't fit the common data model.

Through projecting the complex observation signal into a vector space, we can get a real signal which is can be written as the sum of real sine waves. The projection vector can be anything but a wise option can be the first component of row-wise PCA transform. Because PCA tends to preserve the most powerful components and the first harmonic is always more powerful than the second harmonic. As a result, PCA provides an extra benefit, harmonic suppression.

For example, in the single user case, rows in observation matrix $\overline{\mathbf{X}}$ are nothing but delayed and attenuated versions of the source signal. Fig.4.2 illustrates the PCA transform of such an observation signal. After performing PCA transform, the imaginary part in time domain is the first harmonic in Fig.4.2b and the real part is the second harmonic. By selecting the first principal component, the second harmonic is removed perfectly.

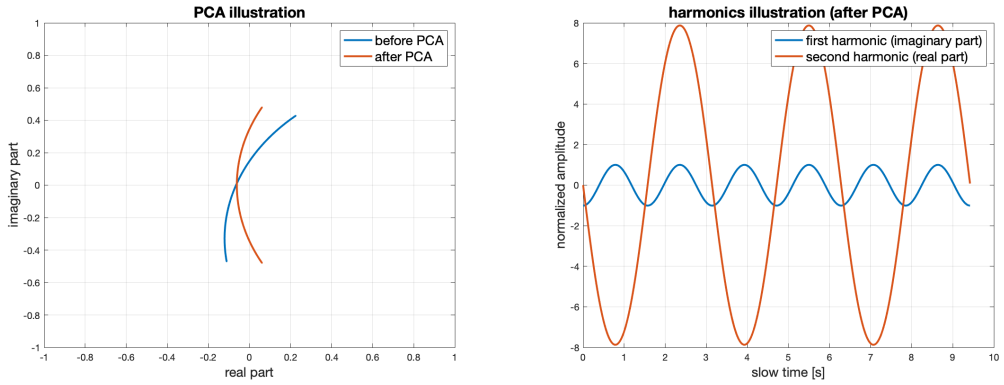


(a) The effect of performing PCA transform to the complex Doppler signal.

(b) Real and imaginary part of Doppler signal after performing PCA

Figure 4.2: PCA transform of single-user case

However, For multi-user case, we can only choose the direction that contains most energy. So we still preserve part of the second harmonics. The signal in the most powerful direction is the summation of projections of the first and second harmonics of two subjects. Generally, after projecting the complex observation vector onto the vector space spanned by the first principal component, we obtain a real signal $\underline{x}_k(m)$

$$\underline{x}_k(m) = \sum_{i=1}^{P} [\alpha_{i,1}(k)\cos(\omega_{r,i} m T_s' + \phi_{r,i}) + \alpha_{i,2}(k)\cos(2\omega_{r,i} m T_s' + 2\phi_{r,i})] \tag{4.11}$$

where $m = 0, 1, \cdots, (M-1)$ and $\alpha_{i,1}(k)$ and $\alpha_{i,2}(k)$ are real coefficient. The Doppler signal is no longer complex after removing the second principle component. In order to factor out the parameters we show no interest in, Hilbert transform is performed to obtain the analytic signal. The Hilbert transform of $\underline{x}_k(m)$ is defined as

$$\begin{aligned} \underline{x}_k^*(m) &= \mathcal{H}\{\underline{x}_k(m)\} \\ &= \sum_{i=1}^{P} [\alpha_{i,1}(k)\sin(\omega_{r,i} m T_s' + \phi_{r,i}) + \alpha_{i,2}(k)\sin(2\omega_{r,i} m T_s' + 2\phi_{r,i})] \end{aligned} \tag{4.12}$$

where $\mathcal{H}\{\cdot\}$ represents the Hilbert transform. So the analytic signal $x_k^A(m)$ is

$$\begin{aligned}\underline{x}_k^A(m) &= \underline{x}_k(m) + j \cdot \underline{x}_k^*(m) \\ &= \sum_{i=1}^{P} \left[\alpha'_{i,1}(k) e^{j\omega_{r,i} m T'_s} + \alpha'_{i,2}(k) e^{j2\omega_{r,i} m T'_s}\right]\end{aligned} \tag{4.13}$$

where $\alpha'_{i,1}(k) = \alpha_{i,1}(k)e^{j\phi_{r,i}}$ and $\alpha'_{i,2}(k) = \alpha_{i,2}(k)e^{j2\phi_{r,i}}$ are complex coefficients. The corresponding data model after applying row-wise PCA transform and Hilbert transform is defined as follows,

$$\underline{\mathbf{X}} = \underline{\mathbf{H}} \cdot \underline{\mathbf{S}} + \mathbf{N} \tag{4.14}$$

where

$$\underline{\mathbf{X}} = \begin{bmatrix} x_0^A(0) & x_0^A(1) & \cdots & x_0^A(M-1) \\ x_1^A(0) & x_1^A(1) & \cdots & x_1^A(M-1) \\ \vdots & \vdots & \ddots & \vdots \\ x_{L-1}^A(0) & x_{L-1}^A(1) & \cdots & x_{L-1}^A(M-1) \end{bmatrix} : L \times M, \tag{4.15}$$

$$\underline{\mathbf{H}} = \left[\begin{array}{ccc|ccc} \alpha'_{1,1}(0) & \cdots & \alpha'_{P,1}(0) & \alpha'_{1,2}(0) & \cdots & \alpha'_{P,2}(0) \\ \alpha'_{1,1}(1) & \cdots & \alpha'_{P,1}(1) & \alpha'_{1,2}(1) & \cdots & \alpha_{P,2}(1) \\ \vdots & \ddots & \vdots & \vdots & \ddots & \vdots \\ \alpha'_{1,1}(L-1) & \cdots & \alpha'_{P,1}(L-1) & \alpha'_{1,2}(L-1) & \cdots & \alpha'_{P,2}(L-1) \end{array}\right] \tag{4.16}$$
$$: L \times 2P,$$

$$\underline{\mathbf{S}} = \left[\begin{array}{cccc} 1 & e^{j\omega_{r,1}T'_s} & \cdots & e^{j\omega_{r,1}(M-1)T'_s} \\ 1 & e^{j\omega_{r,2}T'_s} & \cdots & e^{j\omega_{r,2}(M-1)T'_s} \\ \vdots & \vdots & \ddots & \vdots \\ 1 & e^{j\omega_{r,P}T'_s} & \cdots & e^{j\omega_{r,P}(M-1)T'_s} \\ \hline 1 & e^{j2\omega_{r,1}T'_s} & \cdots & e^{j2\omega_{r,1}(M-1)T'_s} \\ 1 & e^{j2\omega_{r,2}T'_s} & \cdots & e^{j2\omega_{r,2}(M-1)T'_s} \\ \vdots & \vdots & \ddots & \vdots \\ 1 & e^{j2\omega_{r,P}T'_s} & \cdots & e^{j2\omega_{r,P}(M-1)T'_s} \end{array}\right] : 2P \times M, \tag{4.17}$$

$\mathbf{N}$ remains the same because the additive noise is assumed to be white. The model assumptions are summarized as follows,

- $\underline{\mathbf{S}}$ has full row rank $2P$. Each row of $\underline{\mathbf{S}}$ is a complex sine function of slow-time. All the signals are assumed to be random, independent, identically distributed (i.i.d.), with modulus equal to 1.
- The noise is assumed to be additive, white, zero mean, complex Gaussian distributed, with covariance $\mathbf{R}_n = E\{\mathbf{n}\mathbf{n}^H\} = \sigma^2\mathbf{I}$ and be independent from the sources.

## 4.4 The Singular Value Decomposition (SVD)

The $L \times M$ observation matrix $\underline{\mathbf{X}}$ of rank $2P$ has the following SVD [36],

$$\begin{aligned}\underline{\mathbf{X}} &= \underline{\mathbf{U}} \cdot \underline{\mathbf{\Sigma}} \cdot \underline{\mathbf{V}}^{\mathrm{H}} \\ &= \begin{bmatrix}\underline{\mathbf{U}}_{\mathrm{s}} & \underline{\mathbf{U}}_{\mathrm{n}}\end{bmatrix} \left[\begin{array}{ccc|ccc} \sigma_1^2 & & & & & \\ & \ddots & & & & \\ & & \sigma_{2P}^2 & & & \\ \hline & & & \sigma_n^2 & & \\ & & & & \ddots & \\ & & & & & \sigma_n^2 \\ \hline 0 & \cdots & 0 & 0 & \cdots & 0 \\ 0 & \cdots & 0 & 0 & \cdots & 0 \end{array}\right] \begin{bmatrix}\underline{\mathbf{V}}_{\mathrm{s}}^{\mathrm{H}} \\ \underline{\mathbf{V}}_{\mathrm{n}}^{\mathrm{H}}\end{bmatrix}\end{aligned} \tag{4.18}$$

where $\underline{\mathbf{U}}$ is an $L \times L$ unitary matrix, $\underline{\mathbf{V}}$ is an $M \times M$ unitary matrix, $\mathbf{\Sigma}$ is a diagonal matrix whose diagonal elements are singular values of $\underline{\mathbf{X}}$. Columns in $\underline{\mathbf{U}}$ and $\underline{\mathbf{V}}$ are called right and left singular vectors respectively. Singular values are positive real numbers, representing the energy in the corresponding singular vector space. They are ordered such that

$$\sigma_1^2 \geq \sigma_2^2 \geq \cdots \geq \sigma_{2P}^2 \geq \sigma_n^2.$$

The first $2P$ columns of $\underline{\mathbf{U}}$ are denoted as $\underline{\mathbf{U}}_{\mathrm{s}}$, which spans the same column space of $\underline{\mathbf{X}}$. The rest columns of $\underline{\mathbf{U}}$ are denoted as $\underline{\mathbf{U}}_{\mathrm{n}}$, which spans the null space of $\underline{\mathbf{U}}_{\mathrm{s}}$. Similarly, the first $2P$ columns of $\underline{\mathbf{V}}$ is denoted as $\underline{\mathbf{V}}_{\mathrm{s}}$, which spans the same row space of $\underline{\mathbf{X}}$, namely the signal space. $\underline{\mathbf{V}}_{\mathrm{n}}$ is the null space of $\underline{\mathbf{V}}_{\mathrm{s}}$, namely the noise space.

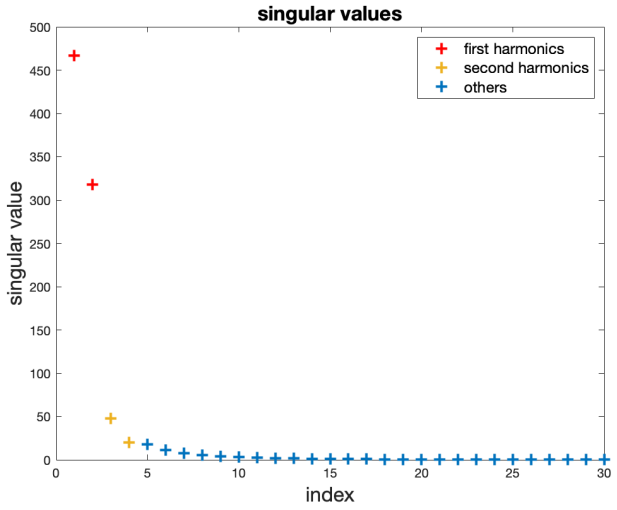


Figure 4.3: Singular values from a practical measurements of two subjects

It is expected to see $P$ comparably large singular values if the second harmonics are suppressed well while to see $P+1$ to $2P$ comparably large singular values if not. An example is shown in Fig.4.3, which is from a practical measurement of 2 subjects.

The first two singular values are much larger than the rest, which means the second harmonics are suppressed very well. Singular values give the power allocation in different singular vector space, based on which, the number of sources can be estimated by identifying the number of dominant singular values.

## 4.5 The MUSIC Algorithm

As mentioned above, the singular values can be utilized to estimate the number of sources. What's more, the singular vectors give the information about the signal space,

$$\text{span}(\underline{\mathbf{V}}_{\text{s}}) = \text{span}(\underline{\mathbf{S}}); \tag{4.19}$$

therefore,

$$\underline{\mathbf{S}} \cdot \underline{\mathbf{V}}_{\text{n}} = 0. \tag{4.20}$$

Given an observation matrix $\underline{\mathbf{X}}$, we can estimate the number of sources $k$ and hence the signal space $\underline{\mathbf{U}}_{\text{s}}$ by selecting the first $2P$ singular vectors as well as the null space$\underline{\mathbf{U}}_{\text{n}}$. Our objective is to estimate the source matrix,

$$\underline{\mathbf{S}} = \begin{bmatrix} \underline{\mathbf{s}}^{\text{H}}(\omega_{r,1}) \\ \vdots \\ \underline{\mathbf{s}}^{\text{H}}(\omega_{r,P}) \\ \underline{\mathbf{s}}^{\text{H}}(2\omega_{r,1}) \\ \vdots \\ \underline{\mathbf{s}}^{\text{H}}(2\omega_{r,P}) \end{bmatrix} \tag{4.21}$$

where the unknown parameters are the respiration frequencies and their second harmonics.

MUltiple SIgnal Classification (MUSIC) is an effective algorithm to estimate the frequencies based on the orthogonality condition in equation 4.20. Since we have

$$\underline{\mathbf{s}}^{\text{H}}(\omega_i)\underline{\mathbf{V}}_{\text{n}} = 0, \quad 1 \leq i \leq 2P, \tag{4.22}$$

the corresponding cost function of MUSIC is

$$\mathcal{J}_{MUSIC} = \frac{||\underline{\mathbf{s}}(\omega)||^2}{||\underline{\mathbf{s}}^{\text{H}}(\omega)\underline{\mathbf{V}}_{\text{n}}||^2}. \tag{4.23}$$

The frequencies corresponds to the first $2P$ largest local maxima of the cost function are chosen as the estimated frequencies. An example of the estimated MUSIC pseudo-spectra from the same measurement in Fig.4.3 are shown in Fig.4.4a and Fig.4.4b when the number of sources is set to 2 and 4 respectively. The ground truth of the respiration frequencies is: $f_{r,1} = 0.2$Hz, $f_{r,2} = 0.26$Hz.

With regard to the results shown in Fig.4.3 and Fig.4.4, we can conclude that after performing PCA, it is for sure that the power of the first harmonics are much larger than the that of the second harmonics. Therefore, it is not necessary to consider the second harmonics in the source matrix $\underline{\mathbf{S}}$. However, to precisely describe the model, we

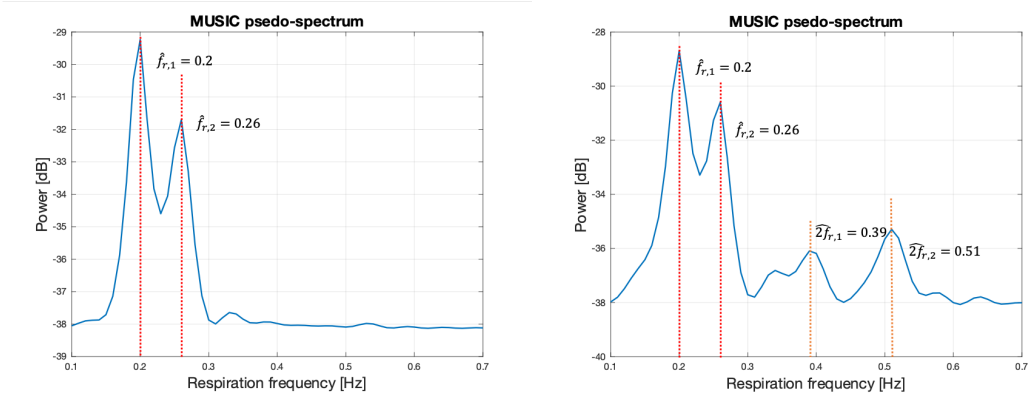


(a) 2 sources (b) 4 sources

Figure 4.4: MUSIC pseudo-spectrum of respiration

can keep the second harmonics in $\underline{\mathbf{S}}$ and then pick $P$ estimated frequencies out of $2P$ estimated ones based on the relationship between the first harmonic and the second harmonic, i.e., the frequency of the second harmonic is twice of the frequency of the first harmonic.

Recall the signal model of physiological activities in equation 2.8 and the source signal model in equation 4.7, if we want to estimate the heartbeat frequency using MUSIC, one option is to extend both the signal space and the steering frequency range. In other words, we also consider the heartbeat signal in $\bar{s}_i(m)$. Then,

$$\begin{aligned}\bar{s}_i(m) \approx\ & j\frac{4\pi f_0}{c}\left[a_{r,i}\cos(\omega_{r,i}mT_s' + \phi_{r,i}) + a_{h,i}\cos(\omega_{h,i}mT_s' + \phi_{h,i})\right] \\ & + \frac{1}{4}\left(\frac{4\pi f_0}{c}\right)^2 a_{r,i}^2\cos\left(2\omega_{r,i}mT_s' + 2\phi_{r,i}\right),\end{aligned} \tag{4.24}$$

$$\underline{\mathbf{S}} = \begin{bmatrix} \underline{\mathbf{s}}^{\mathrm{H}}(\omega_{r,1}) \\ \vdots \\ \underline{\mathbf{s}}^{\mathrm{H}}(\omega_{r,P}) \\ \hline \underline{\mathbf{s}}^{\mathrm{H}}(2\omega_{r,1}) \\ \vdots \\ \underline{\mathbf{s}}^{\mathrm{H}}(2\omega_{r,P}) \\ \hline \underline{\mathbf{s}}^{\mathrm{H}}(\omega_{h,1}) \\ \vdots \\ \underline{\mathbf{s}}^{\mathrm{H}}(\omega_{h,P}) \end{bmatrix} : 3P \times M. \tag{4.25}$$

For instance, let us still consider the same measurement, if we regard the first 6 singular vectors as $\underline{\mathbf{V}}_{\mathrm{s}}$ and scan the frequency from 1Hz to 1.5Hz with step size 0.01Hz, we can obtain a pseudo-spectrum which is shown in Fig.4.5. The corresponding frequencies of the two largest two local maxima are the estimated heartbeat frequencies. The references of heartbeat frequencies are: $f_{h,1} = 1.26$Hz, $f_{h,2} = 1.37$Hz. The estimated results are regarded to be consistent with the references. However, as we can see

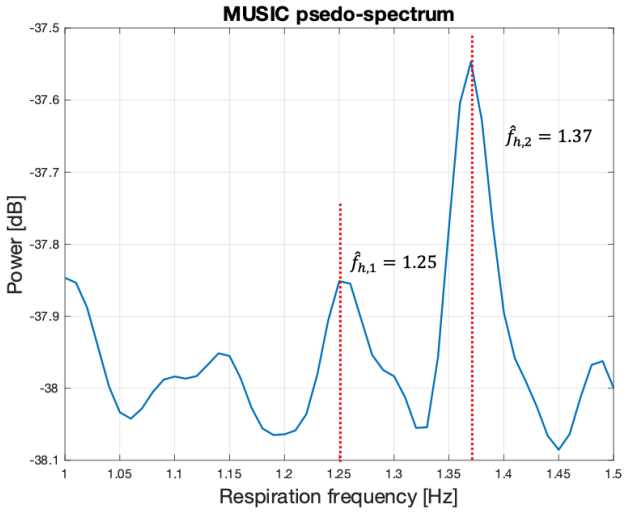


Figure 4.5: MUSIC pseudo-spectrum of heartbeat

from equation 4.7, the heartbeat signal is very weak compared with other components. It is likely that the harmonics fall into the searching range are more dominant than the heartbeat. Another problem of MUSIC algorithm is that for multiple parameter estimation problem, it suffers from the order ambiguity. For two subjects, there are 4 different combinations of respiration frequencies and heartbeat frequencies. Consequently, MUSIC is applicable to single user case instead of multi-user case. A more robust way which is also applicable to multi-user case will be introduced in the next chapter.

# 5 Blind Source Separation

In chapter 3, we derived a general data model for our radar-based health monitoring system, in presence of noise and interference from static clutters, expressed in equation 3.19. In section 4.1, we remove the DC information by multiplying a projection matrix, resulting in a common data model in array signal processing, expressed in equation 4.4. Since the performance of the MUSIC algorithm suffers from the harmonics, a more robust Blind Source Separation (BBS) algorithm, i.e., Independent Component Analysis (ICA), will be proposed in this chapter.

## 5.1 Noise Reduction via SVD

The data model after DC removal is $\overline{\mathbf{X}} = \mathbf{H}\overline{\mathbf{S}} + \mathbf{N}$ where every row of $\overline{\mathbf{S}}$ is an arc, resulting in a complex sinusoidal-like wave which is a linear combination of groups of sine waves with a dominant component, i.e., respiration signal. The statistical independence of common signals are validated in [37]. It has been proved that sine waves of different frequencies are highly independent with each other; therefore, the rows in $\overline{\mathbf{S}}$ can be regarded as independent source signals. The statistics of the above data model are summarized as follows,

- $\overline{\mathbf{S}}$ has full row rank $P$.
- Rows of $\overline{\mathbf{S}}$ are random, independent and i.i.d.
- The noise is additive white Gaussian noise with covariance $\mathbf{R}_n = \sigma^2\mathbf{I}$.

The SVD of $\overline{\mathbf{X}}$ is

$$\begin{aligned}\overline{\mathbf{X}} &= \overline{\mathbf{U}} \cdot \overline{\mathbf{\Sigma}} \cdot \overline{\mathbf{V}}^{\mathrm{H}} \\ &= \begin{bmatrix}\overline{\mathbf{U}}_{\mathrm{s}} & \overline{\mathbf{U}}_{\mathrm{n}}\end{bmatrix} \left[\begin{array}{ccc|ccc} \sigma_1^2 & & & & & \\ & \ddots & & & & \\ & & \sigma_P^2 & & & \\ \hline & & & \sigma_n^2 & & \\ & & & & \ddots & \\ & & & & & \sigma_n^2 \\ \hline 0 & \cdots & 0 & 0 & \cdots & 0 \\ 0 & \cdots & 0 & 0 & \cdots & 0 \end{array}\right] \begin{bmatrix}\overline{\mathbf{V}}_{\mathrm{s}}^{\mathrm{H}} \\ \overline{\mathbf{V}}_{\mathrm{n}}^{\mathrm{H}}\end{bmatrix},\end{aligned} \tag{5.1}$$

where $\overline{\mathbf{U}}$ is an $L \times L$ unitary matrix containing left singular vectors while $\overline{\mathbf{V}}$ is an $M \times M$ unitary matrix containing right singular vectors, $\overline{\mathbf{\Sigma}}$ is a diagonal matrix containing all the singular values. The first $P$ columns in $\overline{\mathbf{U}}$ and $\overline{\mathbf{V}}$ are denoted as $\overline{\mathbf{U}}_s$ and $\overline{\mathbf{V}}_s$

respectively. The rest columns are denoted as $\overline{\mathbf{U}}_n$ and $\overline{\mathbf{V}}_n$ respectively. Indeed, columns of $\overline{\mathbf{V}}_s$ span the same subspace as rows in $\overline{\mathbf{S}}$ and columns of $\overline{\mathbf{V}}_n$ span the null pace as rows in $\overline{\mathbf{S}}$. Hence, $\overline{\mathbf{V}}_s$ can be expressed as the following linear transform [36],

$$\overline{\mathbf{V}}_s = \mathbf{A}\overline{\mathbf{S}}, \tag{5.2}$$

where $\mathbf{A}$ is a $P \times P$ square mixing matrix. In this way, the noise falls into the null space of the signal subspace can be removed totally.

## 5.2 The ICA Algorithm

In equation 5.2, rows of $\overline{\mathbf{S}}$ are underlying sources, $\mathbf{A}$ is a mixing matrix and rows of $\overline{\mathbf{V}}_s$ are mixtures of sources in $\overline{\mathbf{S}}$. This data model is consistent with the classical cocktail-party problem in [38]. Such kind of BBS problem can be addressed by ICA. According to [39], the restrictions of applying ICA are,

- the source signals are non-Gaussian distributed,
- the source signals are statistically independent,
- the mixing matrix is square.

Since the rows of $\overline{\mathbf{S}}$ are sinusoidal-like waves, it is for sure that the sources are non-Gaussian distributed. The independence of sources are discussed in section 5.1. Thus, our data model satisfies all the restrictions. Intuitively, the inverse of $\mathbf{A}$ is the unmixing matrix we look for. While both $\overline{\mathbf{S}}$ and $\mathbf{A}$ are unknowns, ICA seeks an unmixing matrix $\mathbf{W}$ that maximizes the statistical independence of each source [37].

Based on the central limit theorem, the sum of independent random variables tend to a Gaussian distribution. This gives us the inspiration that the estimated independent sources should tend to be as non-Gaussian distributed as possible. According to [39], there are plenty of metrics to measure the non-Gaussianity of $\overline{\mathbf{S}}$, such as the maximum likelihood, kurtosis, negentropy and mutual information, leading to different objective functions.

Maximum likelihood requires the probability density distribution of the source signal or a family of simple approximations of the density functions. Estimators of higher-order cumulants using finite samples are very sensitive to outliers. Besides, higher-order cumulants mainly measure the tails of the distribution, ignoring the density structure around the center of the distribution [39]. For uncorrelated sources with unit variance, the cost functions of mutual information and negentropy differ only by a sign and a constant [38]. Above all, we choose negentropy as the measure of non-Gaussianity.

Negentropy $\mathcal{J}_{Neg}$ of a complex random vector $\psi$ is defined as [40],

$$\mathcal{J}_{Neg}(\psi^I, \psi^R) = H(\psi^R_{gauss}, \psi^I_{gauss}) - H(\psi^I, \psi^R) \tag{5.3}$$

where $\psi_{gauss}$ is a Gaussian random variable with the same covariance matrix as $\psi$ and $H(\cdot)$ represents the differential entropy. Since negentropy requires the prior knowledge of the pdf, nonlinear smooth even functions are used to approximate the negentropy

[40]. The cost function of the fixed-point algorithm for complex signals under the ICA data model is given by [41],

$$\mathcal{J}_{FastICA}(\mathbf{w}) = E\{G(|\mathbf{w}^{\mathrm{H}}\overline{\mathbf{V}}_s|^2)\} \tag{5.4}$$

where $\mathbf{w}$ is an $M$-dimensional unmixing vector,$G_i$ is a is a smooth even function with $G : \mathbb{R}^+ \cup \{0\} \to \mathbb{R}$. The following choices are widely used in practice,

$$G_1(\psi) = \sqrt{a_1 + \psi}, \tag{5.5}$$
$$G_2(\psi) = \log(a_2 + \psi), \tag{5.6}$$
$$G_3(\psi) = \tfrac{1}{2}\psi^2 \tag{5.7}$$

where $a_1$ and $a_2$ are constants. One obtains the following optimization problem,

$$\begin{aligned} &\max_{\mathbf{w}_j} \sum_{j=1}^{P} \mathcal{J}_{FastICA}(\mathbf{w}_j) \\ &\text{subject to } E\{(\mathbf{w}_i^{\mathrm{H}}\mathbf{x})(\mathbf{w}_j^{\mathrm{H}}\mathbf{x})^*\} = \delta_{ij}, \end{aligned} \tag{5.8}$$

where $i$ and $j$ are from 1 to $P$. Then the estimated sources can be obtained by multiplying the unmixing matrix,

$$\widehat{\mathbf{S}} = \mathbf{W}^{\mathrm{H}}\overline{\mathbf{V}}_s, \tag{5.9}$$

where $\mathbf{W}$ is the matrix containing all $\mathbf{w}_j$. The cost function in equation 5.3 only considers the modulus of the the signals for source separation, resulting circular outputs whose structures coincide with our estimated sources in equation 3.18.

Fig.5.1 demonstrates the estimated complex sources by ICA from a practical measurement. As is known to all, independent signals are uncorrelated; therefore, SVD is actually half ICA. However, there is no physical reason for the independent sources to be orthogonal with each other, what ICA does is to optimize the projection angles between the singular vectors and maximize the statistical independence. Similarly, ICA also suffers from the order ambiguity but the difference with MUSIC algorithm is that the heartbeat and respiration signal from the same target are still preserved in one Doppler signal. The way to recover the subject order will be covered in the next chapter.

## 5.3 Phase Demodulation

Latent sources estimated in section 5.2 are the zero mean Doppler signals whereas our signal of interest is the phase information of the Doppler signals. The DC removal step in section 4.1, removes all the DC information, resulting in direct angle extraction unfeasible.

### 5.3.1 Arctangent Demodulation

An intuitive way to demodulate the phase is to recover the DC information and then extracting the phase. Recall the zero mean Doppler signal model in equation 3.18, each

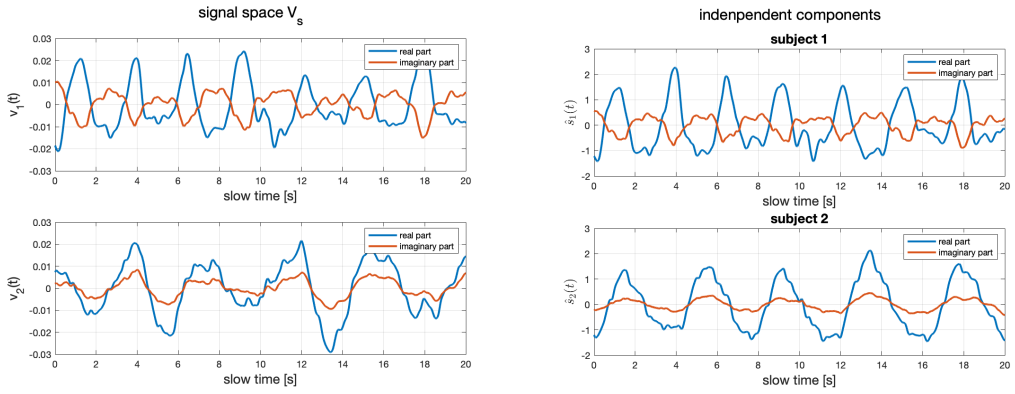


(a) Signal space (b) Independent components

Figure 5.1: Estimated sources by ICA

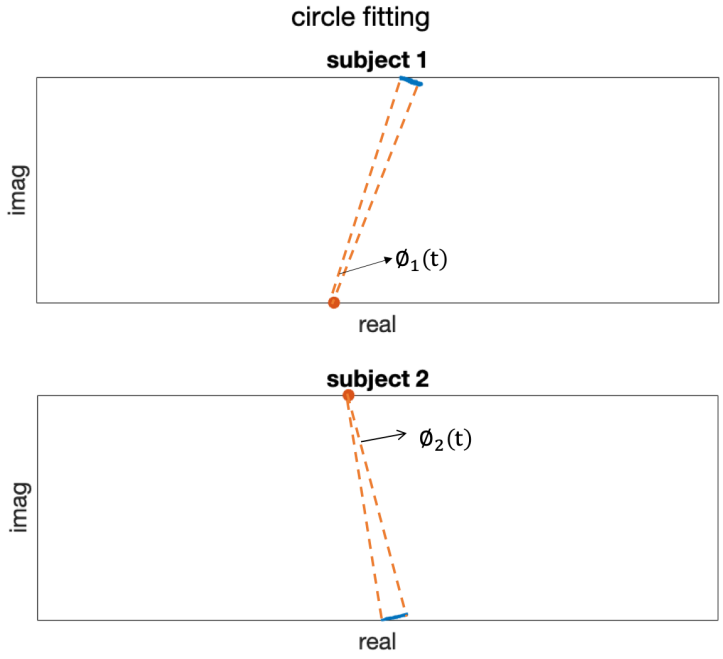


Figure 5.2: Circle fitting

Doppler signal forms an arc in the complex plane. Fig.5.2 illustrate the samples of the estimated sources in Fig.5.1b in an IQ plane

The corresponding center and radius of an arc can be estimated by resolving a non-linear least-squares geometric fitting problem [42]. Assume $\hat{\mathbf{s}}_i$ is the sample vector of $i$-th estimated Doppler signal, $\mathbf{z}_i$ and $r_i$ are the center and radius of the corresponding

circle respectively, the objective function becomes

$$\begin{aligned} \min_{\mathbf{z}_i, r_i} \quad & \sum_{j=0}^{M-1} D_j(\mathbf{z}_i, r_i) \\ \text{subject to } & D_j = (||\mathbf{z}_i - \hat{\mathbf{s}}_{i,j}|| - r_i)^2, \end{aligned} \tag{5.10}$$

where $D_j$ represents the geometry distance between $j$-th sample and the circle. The best circle is iteratively computed then. A good starting vector is the solution of minimizing the algebraic distance [42]. Assume $\mathbf{\Theta}_i = [\hat{\mathbf{s}}_i^R, \hat{\mathbf{s}}_i^I]$, The algebraic representation of a circle is defined as

$$F(\boldsymbol{\theta}_i) = a\boldsymbol{\theta}_i^{\mathrm{T}}\boldsymbol{\theta}_i + \mathbf{b}^{\mathrm{T}}\boldsymbol{\theta}_i + c = 0 \tag{5.11}$$

where $a$ is a nonzero number, $\boldsymbol{\theta}_i$, $\mathbf{b} \in \mathbb{R}^2$ and $\boldsymbol{\theta}_i^T$ is a row of $\mathbf{\Theta}_i$. Given the sample matrix $\mathbf{\Theta}_i$, we can compute the circle parameters, $\hat{a}, \hat{\mathbf{b}}, \hat{c}$. Only when all the samples are on one circle can we find a unique solution. Otherwise, it is an overdetermined problem when the sample length is more than 3. Let $\boldsymbol{\eta}_i = [a, b_1, b_2, c]^T$ and $\mathbf{B}_i = [\mathbf{\Lambda}_i\mathbf{\Lambda}_i^T, \mathbf{\Lambda}_i, \mathbf{1}]$, equation 5.11 can be converted into a linear equation $\mathbf{B}_i\boldsymbol{\eta}_i = \mathbf{0}$. The non-trival solution can be obtained by solving the following standard optimization problem,

$$\begin{aligned} &\min ||\mathbf{B}_i\boldsymbol{\eta}_i|| \\ &\text{subject to} ||\boldsymbol{\eta}_i|| = 1. \end{aligned} \tag{5.12}$$

Then the center and the radius can be computed:

$$\mathbf{z}_i = \left(-\frac{b_1}{2a}, -\frac{b_2}{2a}\right) \quad r_i = \sqrt{\frac{||\mathbf{b}||^2}{4a^2} - \frac{c}{a}}. \tag{5.13}$$

After knowing the coordinates of the center, the arc can be shifted back to where it was. As a result, we can demodulate the phases by directly computing the angles of the complex values. According to equation 2.11, the chest surface motion is obtained as,

$$\hat{y}_i(t) = \frac{4\pi f_0}{c}\phi_i(t) = \tan^{-1}\left(\frac{\hat{\mathbf{s}}_i^I(t) - z_{i,1}}{\hat{\mathbf{s}}_i^R(t) - z_{i,2}}\right) \cdot \frac{4\pi f_0}{c} \tag{5.14}$$

which is known as arctangent demodulation [13]. Examples of the demodulated phases from the same measurement used in Fig.5.2 are shown in Fig.5.3. As derived in equation 2.8, $y(t)$ consists of a strong respiration signal and a comparably much weaker heartbeat signal. Clearly we can see in Fig.5.3 the respiration is the most dominant component and heartbeat is more obvious during the transition period between inhalation and exhalation.

### 5.3.2 Linear Demodulation

Another way to do phase demodulation is based on the Taylor expansion we discussed in section 4.2. Based on small angle approximation which is the case in our project as is shown in Fig.5.2, the Doppler signal can be approximated as,

$$\begin{aligned} s_i(t) &= e^{j\phi_i(t)} \\ &\approx 1 + j\phi_i(t) - \frac{\phi_i^2(t)}{2}. \end{aligned} \tag{5.15}$$

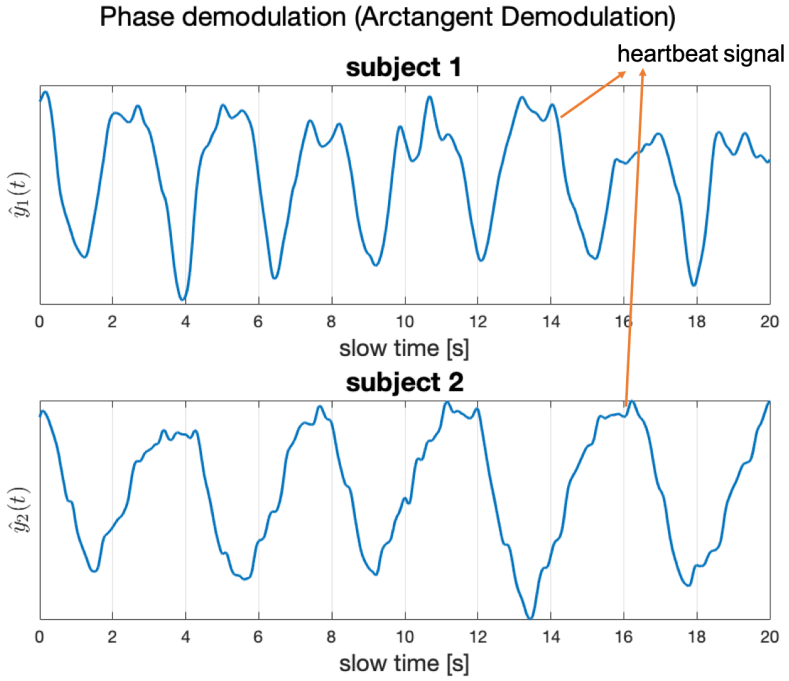


Figure 5.3: Demodulated phases by arctangent demodulation

From equation 4.7, we know that the quadratic term in equation 5.15 consists of the second harmonics and a constant. Therefore, $s_i(t)$ can be rewritten as,

$$s_i(t) \approx s_i^{DC} + j\phi_i(t) + \gamma_i(t), \tag{5.16}$$

where $\gamma_i(t)$ includes the sine waves with angular frequencies: $2\omega_{r,i}, 2\omega_{h,i}, \omega_{r,i} - \omega_{h,i}, \omega_{r,i} + \omega_{h,i}$ and $s_i^{DC}$ is the DC component of $s_i(t)$. Hence, the estimated zero-mean complex source $\hat{s}_i(t)$ can be modeled as

$$\hat{s}_i(t) = j\phi_i(t) + \gamma_i(t) \tag{5.17}$$

where the imaginary part is more powerful than the real part and they are orthogonal with each other. Let $\underline{\hat{\mathbf{s}}}_i = [\hat{\mathbf{s}}_i^R, \hat{\mathbf{s}}_i^I]$, the most powerful component can be found by PCA. The SVD of $\underline{\hat{\mathbf{s}}}_i$ is defined as,

$$\underline{\hat{\mathbf{s}}}_i = [\mathbf{u}_1, \mathbf{u}_2] \cdot \begin{bmatrix} \sigma_1 & \\ & \sigma_2 \end{bmatrix} \cdot [\mathbf{v}_1, \mathbf{v}_2]^{\mathrm{H}}, \tag{5.18}$$

where $\mathbf{u}_1$ and $\mathbf{u}_2$ are left singular vectors, $\mathbf{v}_1$ and $\mathbf{v}_2$ are right singular vectors, $\sigma_1$ and $\sigma_2$ are positive real singular values with $\sigma_1 > \sigma_2$. By projecting the $\underline{\hat{s}}_i(t)$ on to the most powerful direction, i.e., the vector space spanned by $\mathbf{v}_1$, we can obtain the estimated phase $\hat{\phi}_i(t)$. Therefore, the chest surface motion can be estimated as,

$$\hat{y}_i(t) = \frac{4\pi f_0}{c} \underline{\hat{\mathbf{s}}}_i \cdot \mathbf{v}_1. \tag{5.19}$$

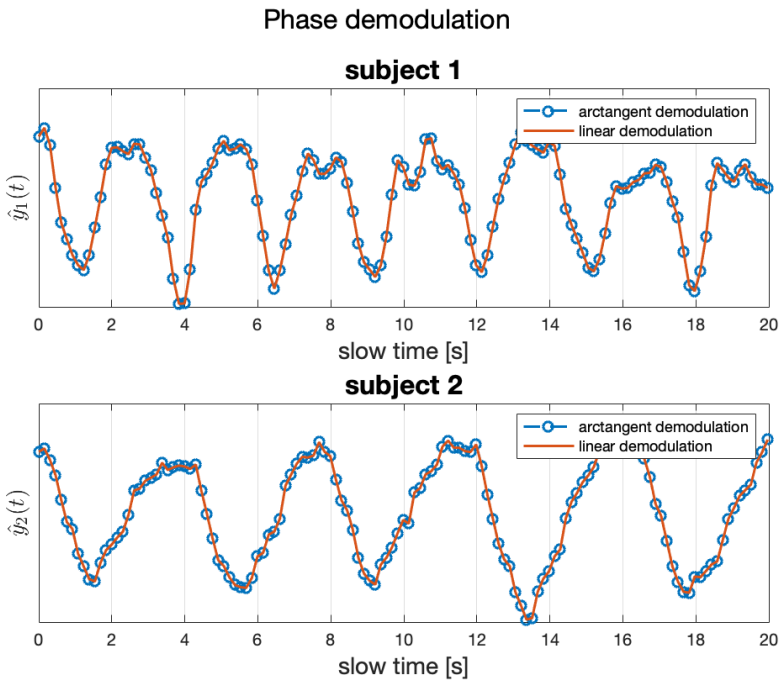


Figure 5.4: Demodulated phases by linear demodulation

An example is shown in Fig.5.4, which is very similar with the result obtained by arctangent demodulation. The advantages of performing linear demodulation are: first, it is faster than circle fitting; second, it is more robust in presence of outliers.

## 5.4 Generalized Line Spectral Estimation

Conventionally, FFT is used for frequency estimation problem. However, the resolution of FFT depends on the observation time; therefore, FFT is not popular for real time application. Parametric methods such as MUSIC [43] and ESPRIT (Estimation of signal parameters via rotational via rotational invariance) [44] are array signal processing algorithms, requiring multiple observations. The chest surface motion $y(t)$ can be regarded as the sum of sinusoidal waves. [45] proposed a generalized line spectral estimation algorithm to estimate both frequencies and amplitudes of a mixture of few sinusoidal signals. This approach can be applied to recover signals that are sparse in continuously indexed dictionaries. In practice, the parameter space is a discretized continuous parameter space which introduces gridding error. However, as long as the step size of the parameter space is chosen to be sufficiently fine, the gridding error can be negligible. Such kind of signal reconstruction problem can be converted into a quadratic smoothing problem [46] and solved by convex optimization tools.

### 5.4.1 Respiration Frequency Estimation

The first step of frequency estimation is to generate the analytic signal. The Hilbert transform of $\hat{y}_i(t)$ is defined as,

$$\begin{aligned} \hat{y}_i^*(t) &= \mathcal{H}(\hat{y}_i(t)) \\ &= a_h \sin(\omega_h t + \phi_h) + a_r \sin(\omega_r t + \phi_r), \end{aligned} \tag{5.20}$$

The analytic signal $\hat{y}_i^A(t)$ is then

$$\begin{aligned} \hat{y}_i^A(t) &= \hat{y}_i(t) + j \cdot \hat{y}_i^*(t) \\ &= a_{h,i} \cos(\omega_{h,i} t + \phi_{h,i}) + a_{r,i} \cos(\omega_{r,i} t + \phi_{r,i}) \\ &+ j \cdot a_{h,i} \sin(\omega_{h,i} t + \phi_{h,i}) + j \cdot a_{r,i} \sin(\omega_{r,i} t + \phi_{r,i}) \\ &= a_{h,i} e^{j\phi_{h,i}} e^{j\omega_{h,i} t} + a_{r,i} e^{j\phi_{r,i}} e^{j\omega_{r,i} t} \\ &= a_{h,i} e^{j\phi_{h,i}} e^{j2\pi f_{h,i} t} + a_{r,i} e^{j\phi_{r,i}} e^{j2\pi f_{r,i} t}. \end{aligned} \tag{5.21}$$

The benefit of using analytic signal is that the amplitude and the initial phase can be factored out, as a result, the only parameter to be estimated is frequency. Equation 5.21 can be rewritten into a matrix form as $\hat{\mathbf{y}}_i^A = \boldsymbol{\lambda}_i^{\mathrm{H}} \mathbf{f}$, where

$$\mathbf{f} = [e^{j2\pi f_{min} t}, e^{j2\pi (f_{min} + \Delta f) t}, e^{j2\pi (f_{min} + 2\Delta f) t}, \cdots, e^{j2\pi f_{max} t}]^{\mathrm{H}}, \tag{5.22}$$

$\boldsymbol{\lambda}_i$ is an unknown vector which indicates the complex weights of the sinusoidal candidates in $\mathbf{f}$, $\Delta f$ is the resolution of the discretized dictionary. To estimate $\boldsymbol{\lambda}_i$ from the estimated complex vital sign $\hat{\mathbf{y}}_i^A$, we can convert the estimation problem into a convex optimization problem of the form,

$$\min_{\boldsymbol{\lambda}_i} \quad ||\hat{\mathbf{y}}_i^A - \boldsymbol{\lambda}_i^{\mathrm{H}} \mathbf{f}||_2^2 + \zeta ||\boldsymbol{\lambda}_i||_1 \tag{5.23}$$

where $\zeta$ is a positive real value and the $l$-1 norm term is added to preserve the sparsity of the weight vector. Based on the prior knowledge about respiration, we know that the respiration frequency range is from 0.1Hz to 0.8Hz. Since the heartbeat signal is very weak compared with the respiration signal, we can assume $y_i(t) \approx a_{r,i} e^{j\phi_{r,i}} e^{2\pi f_{r,i} t}$. Therefore, we can temporally focus on frequencies between 0.1Hz and 0.8Hz to reconstruct $\hat{\mathbf{y}}_i^A$. Fig.5.5 illustrate an estimated weight vectors and the reconstructed respiration signals. The ground truth of respiration frequencies are: $f_{r,1} = 0.36$Hz, $f_{r,2} = 0.24$Hz.

### 5.4.2 Heartbeat Frequency Estimation

To prevent the strong respiration signal from burying the weak heartbeat signal, it would be wise to estimate the parameters (i.e., respiration frequency $\hat{f}_r$ and heartbeat frequency $\hat{f}_h$) iteratively [47]. That is to say, we can estimate the stronger one first and remove it form the mixture to reveal the weak sinusoidal signal, heartbeat. Let $\hat{y}_{r,i}(t)$ denote the reconstructed respiration signal, we can estimated the heartbeat as,

$$\hat{y}_{h,i}(t) = \hat{y}_i^A(t) - \hat{y}_{r,i}(t). \tag{5.24}$$

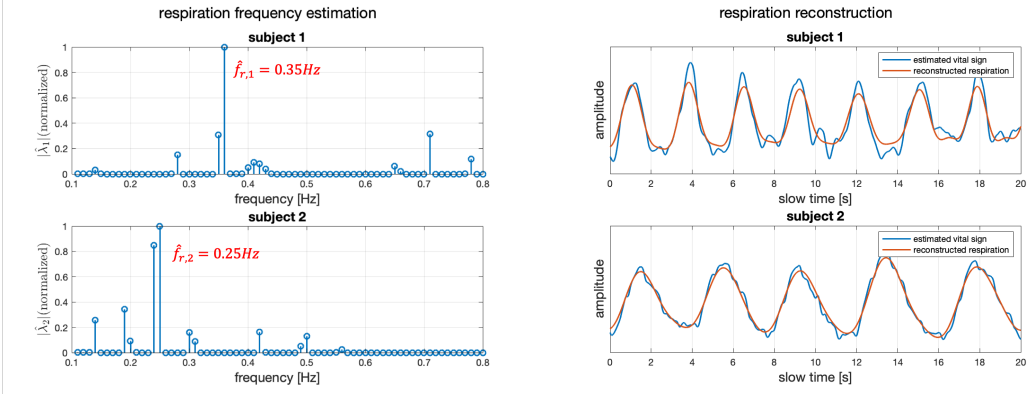


(a) Weight vector estimation ($\zeta$=20) (b) Reconstructed respiration

Figure 5.5: Respiration frequency estimation

For instance, if we subtract the reconstructed respiration signals in Fig.5.5b from the corresponding estimated vital signs, the heartbeat signal will be revealed as is shown in Fig.5.6a. Same methodology in equation 5.23 is applied to estimate the heartbeat frequencies but the frequency range differs,

$$\min_{\boldsymbol{\lambda}_i} \quad ||\hat{\mathbf{y}}_{h,i} - \boldsymbol{\lambda}_i^{\mathrm{H}}\mathbf{f}||_2^2 + \zeta||\boldsymbol{\lambda}_i||_1. \tag{5.25}$$

The estimated result is shown in Fig.5.6b The ground truth of heartbeat frequencies are: $f_{h,1} = 1.14$Hz and $f_{h,2} = 1.17$.

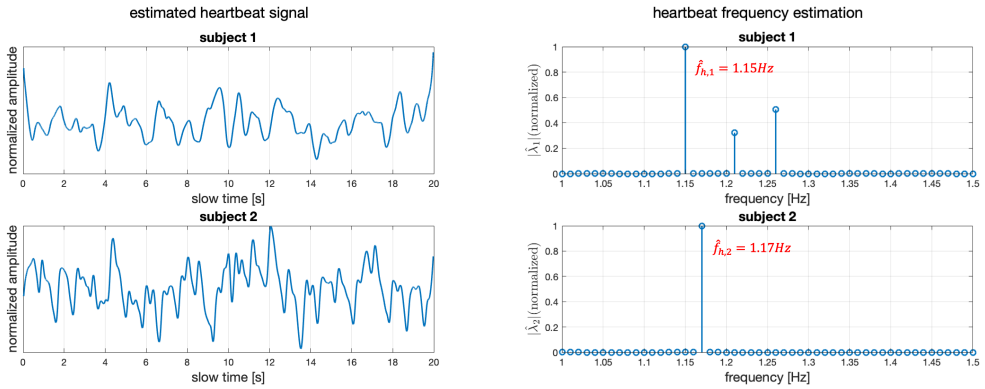


(a) Estimated heartbeat signal (b) Weight vector estimation($\zeta = 5$)

Figure 5.6: Heartbeat frequency estimation

# 6 Indoor Positioning

In equation 4.4, we derived the data model after DC removal, which cancels the interference from static clutters while still preserves the physiological motions of the subjects. $\overline{\mathbf{S}}$ is the source matrix whose estimator is $\hat{\mathbf{S}}$ in equation 5.9. Since we have the noisy observation matrix $\overline{\mathbf{X}}$ and the estimated source matrix $\hat{\mathbf{S}}$, it is possible to estimate $\mathbf{H}$ which contains the channel information, range and attenuation, making it possible to locate the subjects in the room. With $\hat{\mathbf{S}}$ known, we estimate $\mathbf{H}$ by minimizing the residual error,

$$\min_{\mathbf{H}} ||\overline{\mathbf{X}} - \mathbf{H}\hat{\mathbf{S}}||_2 + \zeta||\mathbf{H}||_1, \tag{6.1}$$

where the $l$-1 norm regularization term is added to preserve the sparsity of the multipath propagation channel. Fig.6.1 below is an estimated propagation channel $\hat{\mathbf{H}}$ from a practical measurement (with observation time 20s) where the two subjects are at 1.07m and 2.26m respectively.

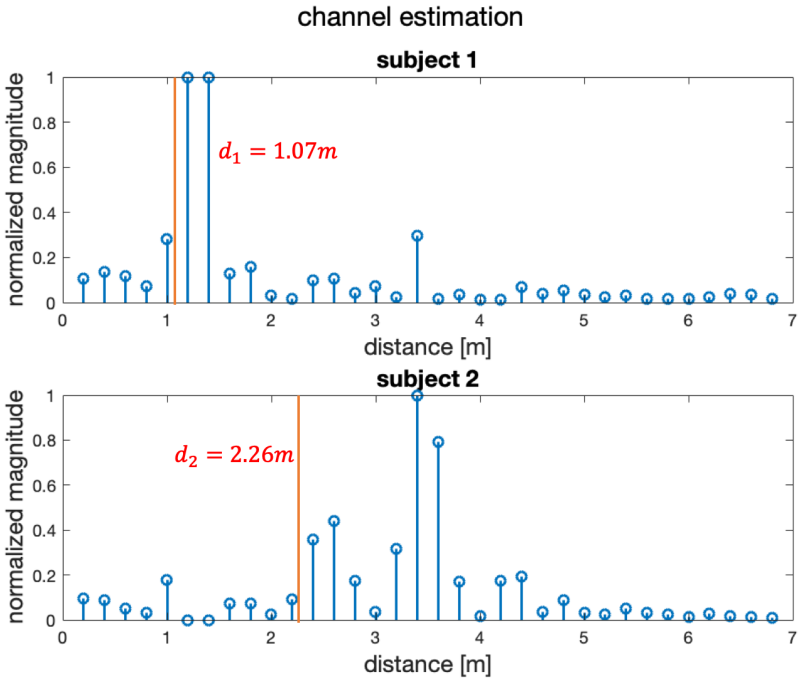


Figure 6.1: Estimated channel ($\zeta = 8$)

Due to the multipath interference from the first subject, vital signs around 2.26m might be disrupted; therefore, we achieve a higher peak at 3.4m, making it more difficult

for indoor positioning of the second subject. With both $\hat{\mathbf{H}}$ and $\hat{\mathbf{S}}$ known, we can remove the order ambiguity resulting from ICA.

# 7 Experimental Validation

The experiments were conducted at imec-NL. All the volunteers are employees, interns, students having a contract with imec-NL. The system used for remote and ono-invasive long-term health monitoring is based on UWB radar technology. In addition, a reference device is used which records contact PPG (photoplethysmogram) signals using a finger clip as well as respiration signals using piezo-resistive sensor on a belt.

## 7.1 Experimental System

### 7.1.1 System for the Radar-based Measurement

The Doppler signals (containing the vital signs information) are obtained by using imec's radar system which consists of a sensor (Fig.7.1), combining radar and computational features, and a base station for a data processing/storage.


Figure 7.1: Radar-based sensor to be used in the acquisition of the Doppler signals

An FMCW radar signal is generated and sent to the subject, and then its reflected echo, containing the vital signs information, is collected by the receiver. The resulting based signals (Doppler signals) are digitized and transmitted through a cable to a base station that consists of a laptop.

### 7.1.2 System for the Reference Measurement

With the aim of obtaining simultaneous reference data in terms of Heartbeat Rate (HR) and Respiration Rate (RR), the g.USBamp device (CE-certified and FDA cleared medical device) (Fig.7.2a) is used to measure both contact PPG and respiration respectively. The respiratory activity is measured from a piezo-resistive sensor placed in a belt also shown in Fig.7.2b, which is placed around the subject's abdomen as is shown in Fig.7.3. The PPG measurement is performed using a compact and lightweight plethysmographic pulse sensor with finger transducer.

(a) g.USBamp device

(b) Belt respiratory sensor

(c) PPG sensor

Figure 7.2: g.USBamp devices and sensors

### 7.1.3 System Setup for Vital Signs Monitoring

The validation was performed in practical room environment (e.g., meeting rooms) of Holst Centre. The real-life environment contains furniture, tables, chairs, metal objects and walls, TVs, white boards, and sofas. Wi-Fi access points also present in the environment.

A high-level block diagram of the experimental set-up is depicted in Fig.7.4. It consists of three main parts: (1) the radar system, (2) the room setting where the volunteers are monitored, and (3) the control system for data acquisition. Separate power supplies are used for the radar, reference system, and data acquisition. The subjects are seated on the chairs and/or sofas, invited to breath normally. The radar system is positioned in the room and is at least 1m away from the subjects. A system operator, who is not in the radar field of view, controls the data acquisition. The

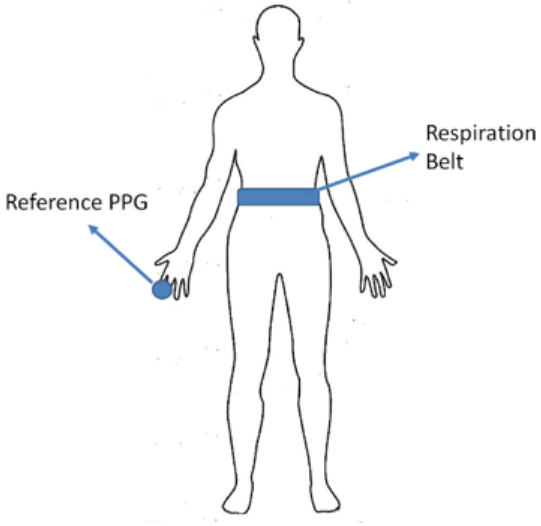


Figure 7.3: Reference sensor placement

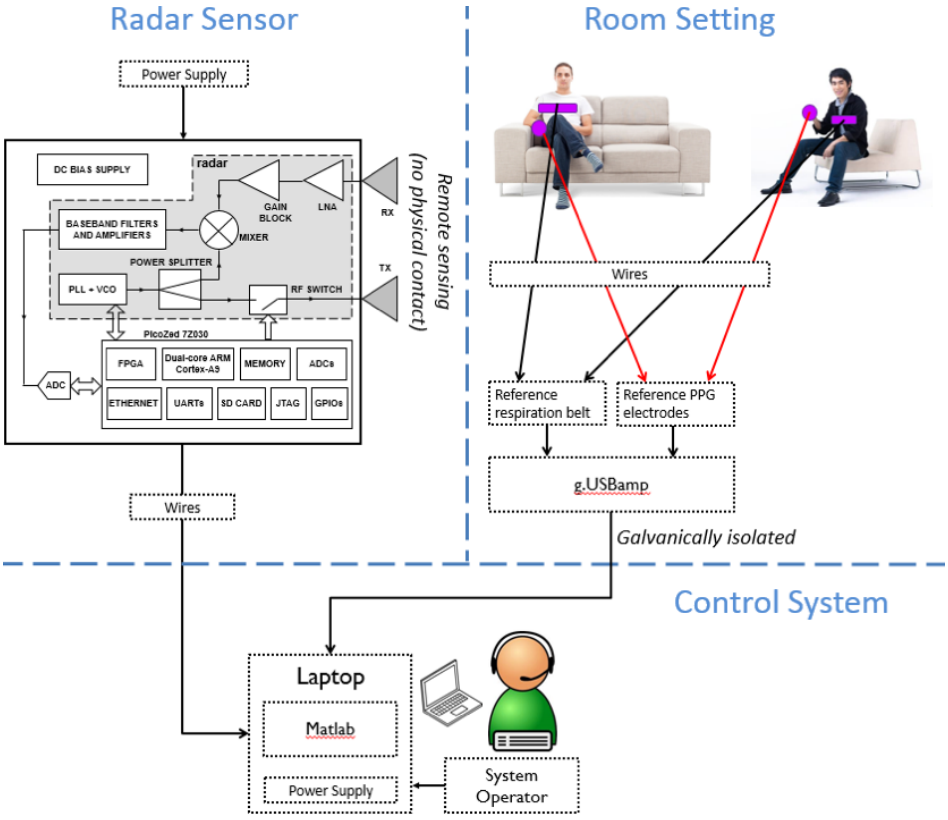


Figure 7.4: Block diagram of the system setup for vital signs monitoring: The radar sensor is not in galvanic contact with the patient and the reference signal circuits are galvanically isolated by the g.USBamp.

reference signals are acquired using the g.USBamp software while the radar signals are acquired using MATLAB.

## 7.2 Experimental Results

All the measurements were collected from two subjects as is shown in Fig.7.5. The subjects are seated at different distances (1m-5m) from the radar with reference sensors on the finger and abdomen. The collected measurements are processed following the advanced data processing steps in Fig.7.6.

Figure 7.5: Experiments conducted in the classroom environment

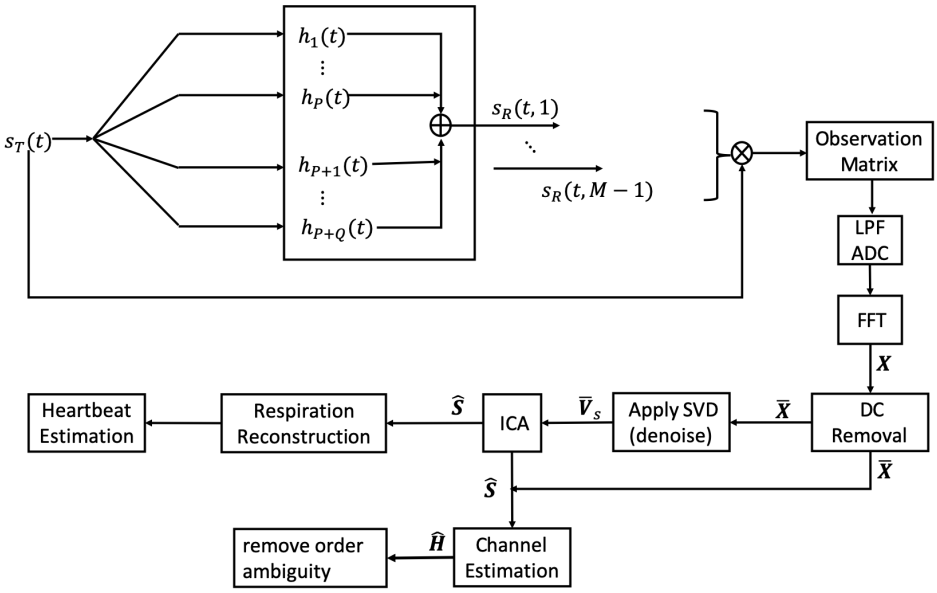


Figure 7.6: Advanced data processing block diagram

Sliding window approach is used to track the vital signs (i.e., HR and RR) and location of the subjects. Fig.7.7 demonstrates the processing result from one of the measurements using linear demodulation and fast-ICA. The observation time of a sliding window is 20s, overlapping of two consecutive windows is 19s. Two subjects are seated at 1.05m and 2.1m respectively. The monitoring lasts 60s in total.

Experiments are repeated for different pairs at different locations, recorded in table 7.1. The overall performance are tested by calculating the success rate of HR and RR (Fig.7.8 and Fig.7.9) and the standard deviation of the location estimation (table 7.2). Here the standard deviation is only calculated for pairs at 1m and 2m because we don't

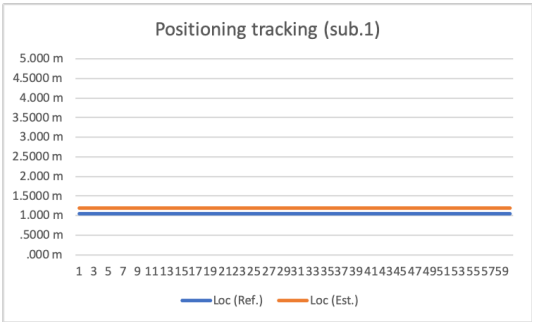


(a) HR tracking of subject 1

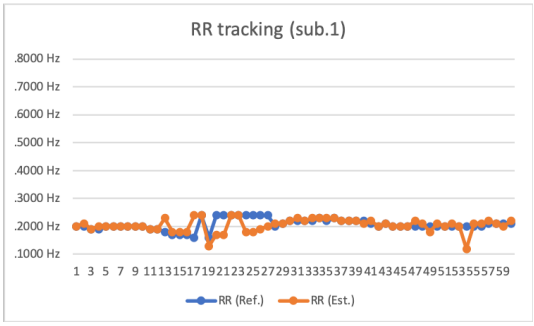


(b) RR tracking of subject 1

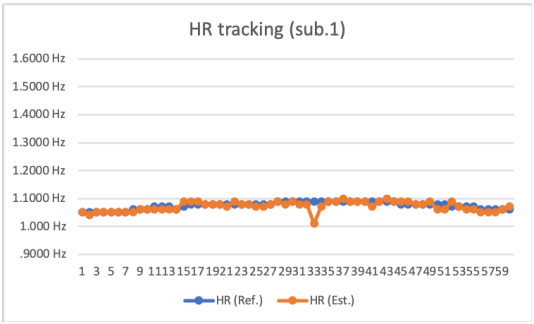


(c) Positioning tracking of subject 1

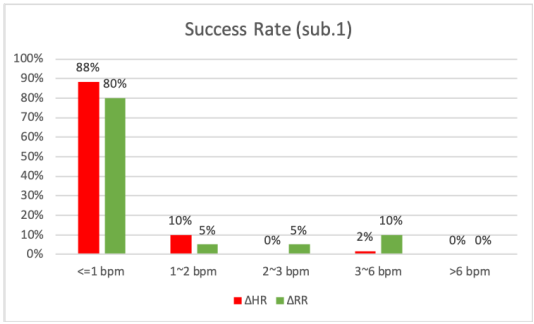


(d) Success rate of subject 1

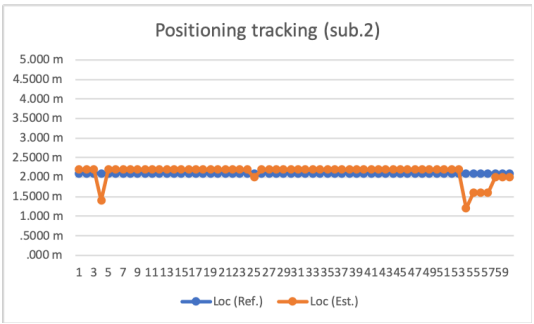


(e) HR tracking of subject 2

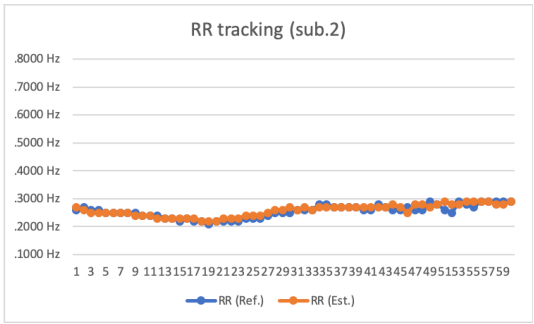


(f) RR tracking of subject 2

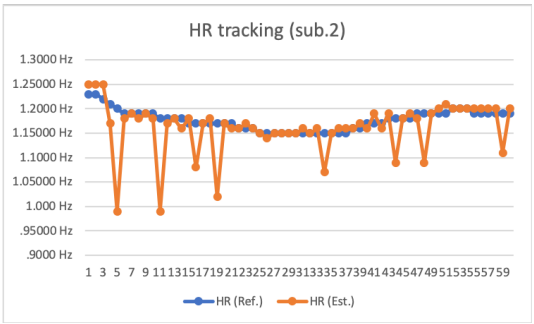


(g) Positioning tracking of subject 2

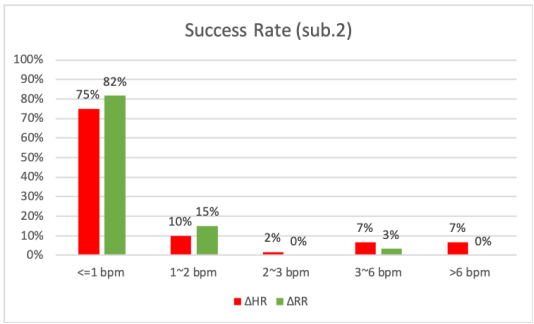


(h) Success rate of subject 2

Figure 7.7: Experimental result of one measurement with window size 20s and step size 1s

have measure the precise distances (from the chestwall of a subject to the antenna) for pairs at other locations. We only know the distance between the seat and the radar which is not the precise path distance. Based on the experimental results, we can

| locations of subjects | 1m/2m | 2m/3.5m | 2m/5m | 3.5m/5m |
|---|---|---|---|---|
| number of pairs | 3 | 4 | 4 | 4 |
| number of measurements for each pair | 4 | 2 | 2 | 2 |

Table 7.1: Experiment recordings

conclude that the the parameter estimations, including positioning, HR and RR are more precise for subjects that are closer to the radar. It makes sense because the closer the subject, the stronger the signal power. The performance of RR tracking doesn't degrade a lot with the increase of the distance between the subject and the radar while it is hard to detect the HR at 5m. Linear demodulation and arctangent demodulation show similar performance in our experiments.

| location of subject | 1m | 2m |
|---|---|---|
| standard deviation (m) | 0.23 | 0.34 |

Table 7.2: Standard deviation of positioning

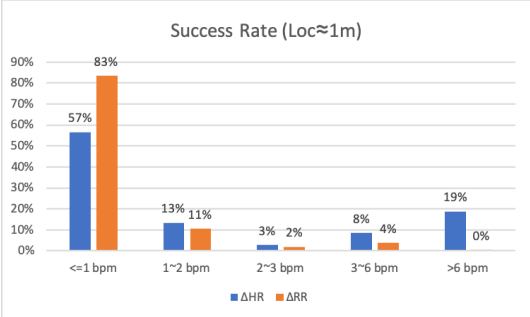


(a) Success rate of sub.1 at 1m

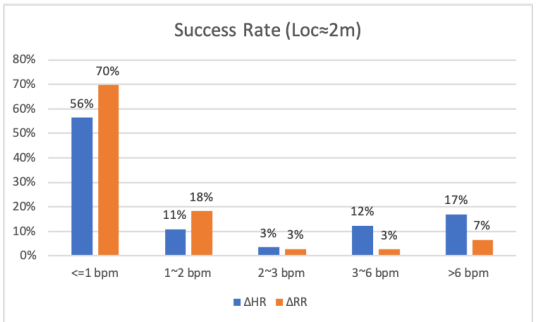


(b) Success rate of sub.2 at 2m

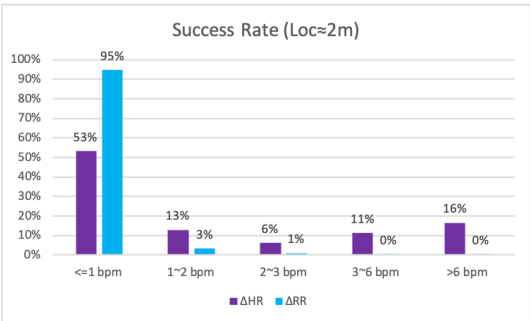


(c) Success rate of sub.1 at 2m

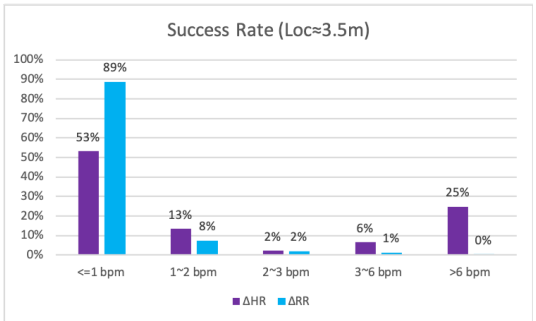


(d) Success rate of sub.2 at 3.5m

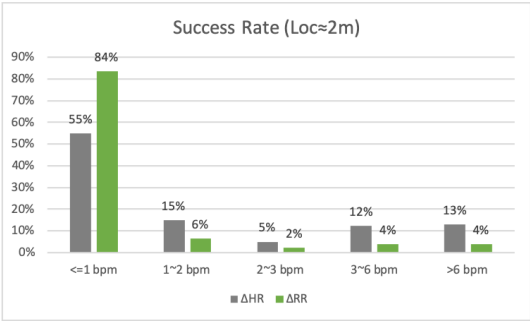


(e) Success rate of sub.1 at 2m

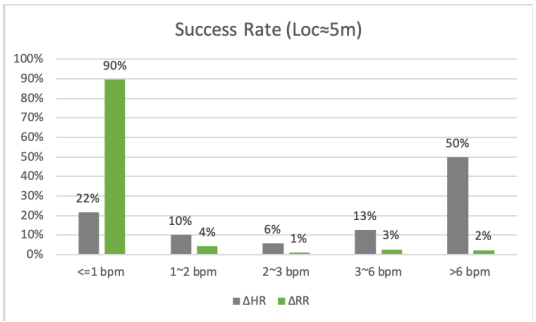


(f) Success rate of sub.2 at 5m

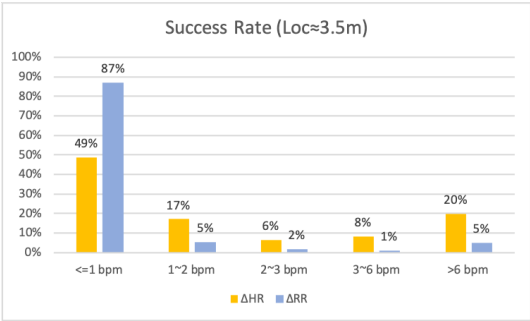


(g) Success rate of sub.1 at 3.5m

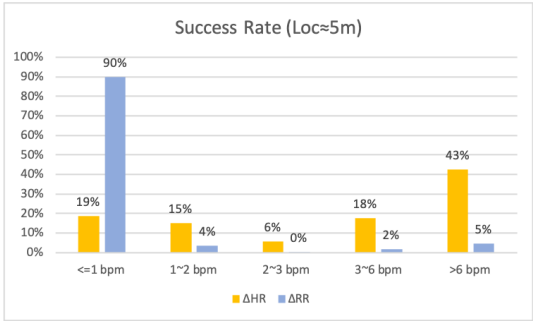


(h) Success rate of sub.2 at 5m

Figure 7.8: Overall performance of vital signs estimation by performing linear demodulation and fast-ICA with window size 20s.

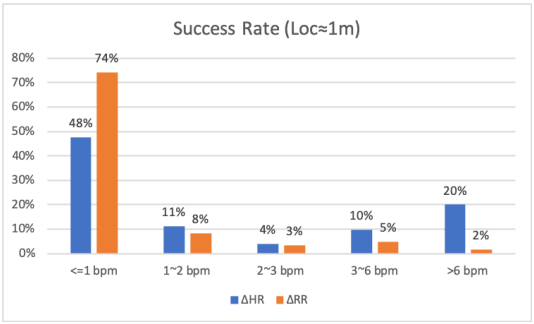


(a) Success rate of sub.1 at 1m

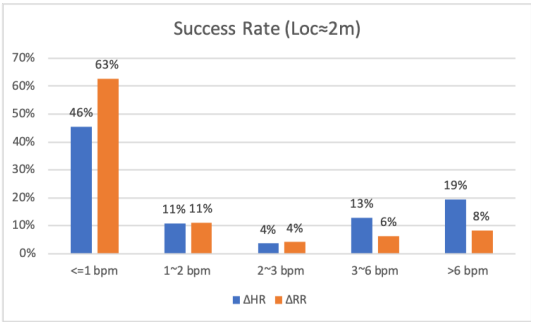


(b) Success rate of sub.2 at 2m

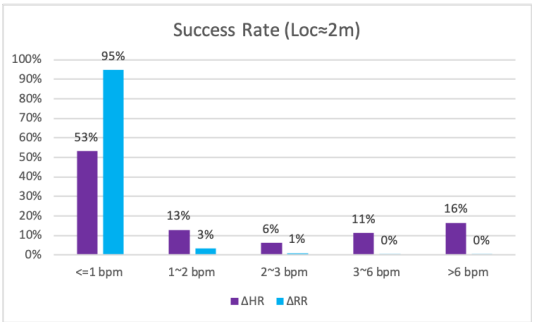


(c) Success rate of sub.1 at 2m

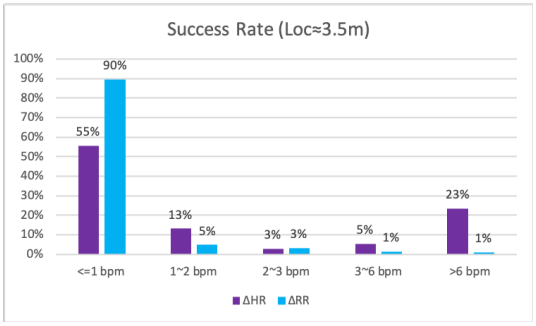


(d) Success rate of sub.2 at 3.5m

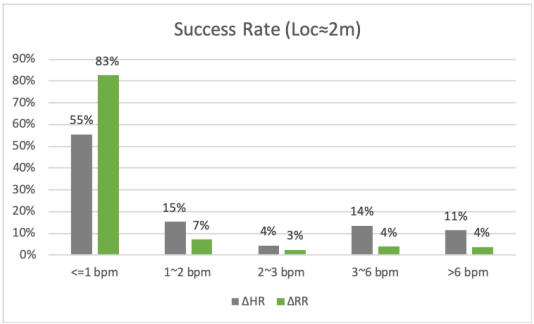


(e) Success rate of sub.1 at 2m

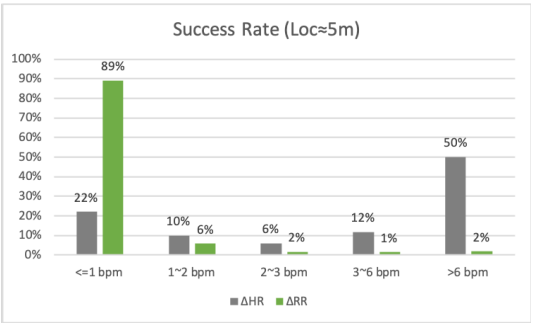


(f) Success rate of sub.2 at 5m

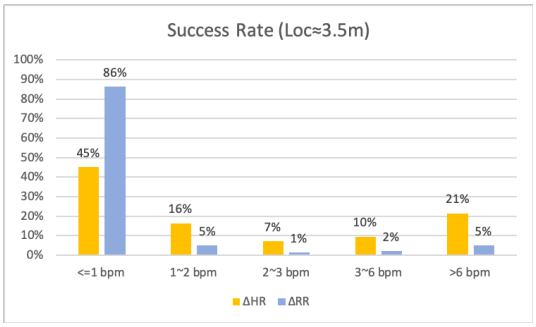


(g) Success rate of sub.1 at 3.5m

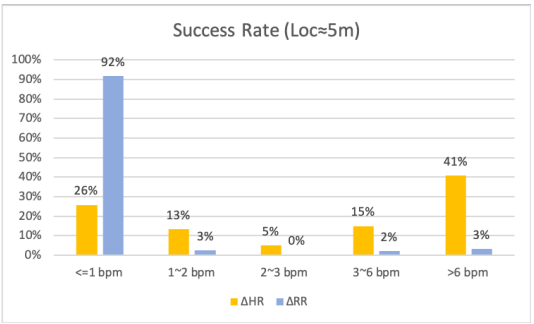


(h) Success rate of sub.2 at 5m

Figure 7.9: Overall performance of vital signs estimation by performing arctangent demodulation and fast-ICA with window size 20s.

# 8 Conclusions and Future Work

## 8.1 Conclusions

The aim of this MSc thesis was to explore the data processing algorithms for radar-based non-contatct long term health monitoring (i.e., HR and RR) and the possibility of realizing indoor positioning at the same time. This is in-line with the growing demand for non-contatct health monitoring in hospitals, schools, homes and cars. More precisely, the objective was multi-parameter estimation based on the precise parametric model we made for the monitoring system. Moreover, by combining with convex optimization approaches, it was possible to track the HR, RR and locations of multiple subjects in real time and in a real indoor environment.

The approaches proposed in the conducted research are borrowed from signal processing for communication but are novel in the related research domain where classical signal processing methods such as wavelet and FFT are widely used to estimated the signals of interests.

The original contributions of this master thesis can be summarized as follows:

- A precise data model were built by taking multipath propagation channel into consideration;
- Clutter suppression by removing the DC information;
- Array signal processing and model based parametric approaches (i.e., MUSIC, ICA, generalized line spectrum estimation) were introduced to cancel the inter-subject interference, overcome the limited resolution of FFT and estimate the parameters of interest.

## 8.2 Future Work

Although based on the experimental results from the practical measurements collected at Holst Centre, the developed data processing algorithms work properly. Further research need to be done to test the robustness of this algorithm by collecting measurements in different room settings and increasing the diversity of volunteers in terms of age, profession, gender, and etc.

The algorithms we used in chapter 4 and chapter 5 are based on the assumptions of second or forth order statistical independence. Algorithms such as constant modulus algorithm (CMA) [48, 49], which have no restrictions about the statistical independence of the signals and make use of the constant modulus property instead, is more motivated based on the source signal model we derived in equation 3.18. Further explorations about CMA is expected to improve the performance of the blind source separation part.

As the performance of applications in indoor environments suffered a lot from the multipath effect. Multiple-input multiple-output (MIMO) radar system is a better option to suppress the inter-subject interference, preventing the Doppler signals from being disrupted by destructive interference. Beamforming or spatial filtering techniques can be used in MIMO system to better improve the indoor positioning [50] and blind source separation [51].

# Bibliography


[1] S. Gulley, E. Rasch, and L. Chan. If we build it, who will come? working-age adults with chronic health care needs and the medical home. *Med. Care*, 49:149155, 2011.

[2] World Health Organization. Global diffusion of ehealth: Making universal health coverage achievable. *Report of the third global survey on eHealth*, 2016.

[3] L Partridge. Gerontology: Extending the healthspan. *Nature*, 529:154, 2016.

[4] C. Levine. Home sweet hospital: the nature and limits of private responsibilities for home health care. *J. Aging Health*, 11:341–359, 1999.

[5] I. Korhonen, J. Parkka, and M. Van Gils. Health monitoring in the home of the future. *IEEE Engineering in Medicine and Biology Magazine*, 22(3):66–73, May 2003.

[6] A Coronato. Uranus: A middleware architecture for dependable aal and vital signs monitoring applications. *Sensors,*, page 31453161, 2012.

[7] D. Schreurs and M. Mercuri. Contactless medical sensing. *2015 IEEE MTT-S International Microwave Symposium,*, pages 1–4, May 2015.

[8] O. Boric-Lubeke and V. M. Lubecke. Wireless house calls: using communications technology for health care and monitoring. *IEEE Microwave Magazine*, 3(3):43–48, Sep. 2002.

[9] C. Li, J. Cummings, J. Lam, E. Graves, and W. Wu. Radar remote monitoring of vital signs. *IEEE Microwave Magazine*, 10(1):47–56, February 2009.

[10] Z. Chen, Y. Liu, S. Li, and G. Wang. Study on the multipath propagation characteristics of uwb signal for indoor lab environments. *2016 IEEE International Conference on Ubiquitous Wireless Broadband (ICUWB),*, pages 1–4, Oct 2016.

[11] Y. Yoon, J. Kim, and Y. Chong. Multipath delay characteristic in mm-wave radio propagation in indoor public area. *2016 International Conference on Information and Communication Technology Convergence (ICTC),*, pages 966–968, Oct 2016.

[12] Q. H. Spencer, B. D. Jeffs, M. A. Jensen, and A. L. Swindlehurst. Modeling the statistical time and angle of arrival characteristics of an indoor multipath channel. *IEEE Journal on Selected Areas in Communications*, 18(3):347–360, March 2000.

[13] G. Wang, C. Gu, T. Inoue, and C. Li. A hybrid fmcw−interferometry radar for indoor precise positioning and versatile life activity monitoring. *IEEE Trans. Microw. Theory Techn.*, 62(11):2812–2822, Nov 2014.

[14] C. Li, Z. Peng, T. Huang, T. Fan, F. Wang, T. Horng, J. Munoz-Ferreras, R. Gomez-Garcia, L. Ran, and J. Lin. A review on recent progress of portable short-range noncontact microwave radar systems. *IEEE Trans. Microw. Theory Techn.*, 65(5):1692–1706, May 2017.

[15] M. Mercuri, Y. H. Liu, I. Lorato, T. Torfs, A. Bourdoux, and C. Van Hoof. Frequency-tracking cw doppler radar solving small-angle approximation and null point issues in non-contact vital signs monitoring. *IEEE Trans. Biomed. Circuits Syst.*, 11(3):671–680, June 2017.

[16] Ilya V. Mikhelson, Sasan Bakhtiari, Thomas W. Elmer, and Alan V. Sahakian. Remote sensing of patterns of cardiac activity on an ambulatory subject using millimeter-wave interferometry and statistical methods. *Med. Biol. Eng. Comput.*, 51(1):135–142, 2013.

[17] M. Mercuri, Y. H. Liu, I. Lorato, T. Torfs, F. Wieringa, A. Bourdoux, and C. Van Hoof. A direct phase-tracking doppler radar using wavelet independent component analysis for non-contact respiratory and heart rate monitoring. *IEEE Trans. Biomed. Circuits Syst.*, 12(3):632–643, June 2018.

[18] C. Li and J. Lin. Random body movement cancellation in doppler radar vital sign detection. *IEEE Trans. Microw. Theory Techn.*, 56(12):3143–3152, Dec 2008.

[19] B. Park, O. Boric−Lubecke, and V. M. Lubecke. Arctangent demodulation with dc offset compensation in quadrature doppler radar receiver systems. *IEEE Trans. Microw. Theory Techn.*, 55(5):1073–1079, May 2007.

[20] A. D. Droitcour, O. Boric-Lubecke, V. M. Lubecke, J. Lin, and G. T. A. Kovacs. Range correlation and i/q performance benefits in single-chip silicon doppler radars for noncontact cardiopulmonary monitoring. *IEEE Trans. Microw. Theory Tech.*, 52(3):838–848, March 2004.

[21] Q. Lv, D. Ye, S. Qiao, Y. Salamin, J. Huangfu, C. Li, and L. Ran. High dynamic−range motion imaging based on linearized doppler radar sensor. *IEEE Trans. Microw. Theory Tech.*, 62(9):1837–1846, Sep. 2014.

[22] F. Wang, C. Li, C. Hsiao, T. Horng, J. Lin, K. Peng, J. Jau, J. Li, and C. Chen. A novel vital−sign sensor based on a self−injection−locked oscillator. *IEEE Trans. Microw. Theory Tech.*, 58(12):4112–4120, Dec 2010.

[23] I Mostafanezhad, E. Yavari, and O. Boric−Lubecke. A low cost simple rf front end using time−domain multiplexing for direction of arrival estimation of physiological signals. *IEEE MTT−S Int. Microw. Symp. Dig.,*, pages 1–4, June 2013.

[24] Z. Peng, J. M. Munoz−Ferreras, Y. Tang, C. Liu, R. Gomez-Garcia, L. Ran, and C. Li. A portable fmcw interferometry radar with programmable low−if architecture for localization, isar imaging, and vital sign tracking. *IEEE Trans. Microw. Theory Techn.*, 65(4):1334–1344, Apr. 2017.

[25] G. Wang, J. Munoz-Ferreras, C. Gu, C. Li, and R. Gomez-Garcia. Application of linear−frequency−modulated continuous-wave (lfmcw) radars for tracking of vital signs. *IEEE Trans. Microw. Theory Techn.*, 62(6):1387–1399, June 2014.

[26] M. Mercuri, P. J. Soh, G. Pandey, P. Karsmakers, G. Vandenbosch, P. Leroux, and D. Schreurs. Analysis of an indoor biomedical radar−based system for health monitoring. *IEEE Trans. Microw. Theory Techn.*, 61(5):2061–2068, May 2013.

[27] Y. H. Liu, S. Sheelavant, M. Mercuri, P. Mateman, J. Dijkhuis, W. Zomagboguelou, A. Breeschoten, S. Traferro, Y. Zhan, T. Torf, C. Bachmann, P. Harpe, and M Babaie. A 680 $\mu$w burst−chirp uwb radar transceiver for vital signs and occupancy sensing up to 15meter distance. *IEEE ISSCC Dig. Tech Papers*, pages 166–167, 2019.

[28] T Sakamoto, R. Imasaka, H. Taki, T. Sato, M. Yoshioka, K. Inoue, T. Fukuda, and H. Sakai. Feature-based correlation and topological similarity for interbeat interval estimation using ultrawideband radar. *IEEE Trans. Biomed. Eng.*, 63(4):747–757, April 2016.

[29] V. Singh, S. Bhattacharyya, and P. K. Jain. Through the wall human signature detection using principle component analysis (pca). *2018 IEEE International Symposium on Antennas and Propagation USNC/URSI National Radio Science Meeting,*, pages 1975–1976, July 2018.

[30] F Adib, H Mao, Z Kabelac, D Katabi, and R C Miller. Smart homes that monitor breathing and heart rate. *ACM CH,*, pages 1–10, 2015.

[31] F Adib, Z Kabelac, and D Katabi. Multi−person localization via rf body reflections. *Usenix NSDI'15,*, pages 279–292, 2015.

[32] Anders Høst-Madsen, Nicolas Petrochilos, Olga Boric-Lubecke, Victor M. Lubecke, Byung-Kwon Park, and Qin Zhou. *Signal Processing Methods for Doppler Radar Heart Rate Monitoring*, pages 121–140. Springer US, Boston, MA, 2008.

[33] Ghufran Shafiq and Kalyana Chakravarthy Veluvolu. Surface chest motion decomposition for cardiovascular monitoring. In *Scientific Reports*, 2014.

[34] A. A. M. Saleh and R. Valenzuela. A statistical model for indoor multipath propagation. *IEEE Journal on Selected Areas in Communications*, 5(2):128–137, February 1987.

[35] William C. Jakes and Donald C. Cox, editors. *Microwave Mobile Communications*. Wiley-IEEE Press, 1994.

[36] V. D. Vrabie and J. I. Mars. Svd-ica: A new tool to enhance the separation between signal and noise subspaces. In *2002 11th European Signal Processing Conference*, pages 1–4, Sep. 2002.

[37] Y Unnisa, D Tran, and F Huang. Statistical independence, measures and testing. 01 2014.

[38] G. D. Clifford. Singular value decompsition & independent component analysis for blind source separation, 2005.

[39] A. Hyvärinen, J. Karhunen, and E. Oja. *Independent Component Analysis*. Adaptive and Cognitive Dynamic Systems: Signal Processing, Learning, Communications and Control. Wiley, 2004.

[40] Michael Novey, Tlay Adal, and Senior Member. Complex ica by negentropy maximization. *IEEE Trans. Neural Netw*, pages 596–609, 2008.

[41] Aapo Hyvrinen. Fast and robust fixed-point algorithms for independent component analysis. *IEEE TRANS. NEURAL NETW*, 10(3):626–634, 1999.

[42] Walter Gander, Gene H. Golub, and Rolf Strebel. Least squares fitting of circles and ellipses, 1994.

[43] P. Gupta and S. P. Kar. Music and improved music algorithm to estimate direction of arrival. In *2015 International Conference on Communications and Signal Processing (ICCSP)*, pages 0757–0761, April 2015.

[44] A. Iozsa and A. Vesa. The esprit algorithm. variants and precision. In *2010 9th International Symposium on Electronics and Telecommunications*, pages 165–168, Nov 2010.

[45] R. Heckel and M. Soltanolkotabi. Generalized line spectral estimation via convex optimization. *IEEE Transactions on Information Theory*, 64(6):4001–4023, June 2018.

[46] Stephen Boyd and Lieven Vandenberghe. Convex optimization, 2004.

[47] Changzhi Li Jenshan Lin. *Microwave Noncontact Motion Sensing and Analysis*. Wiley, September 2013.

[48] A. J. van der Veen and A. Paulraj. An analytical constant modulus algorithm. *IEEE Transactions on Signal Processing*, 44(5):1136–1155, May 1996.

[49] Nicolas Petrochilos, Meriam Rezk, Anders Hst-madsen, Victor Lubecke, and Olga Boric-lubecke. Blind separation of human heartbeats and respiration by the use of a doppler radar remote sensing.

[50] F. Belfiori, W. van Rossum, and P. Hoogeboom. Application of 2d music algorithm to range-azimuth fmcw radar data. In *2012 9th European Radar Conference*, pages 242–245, Oct 2012.

[51] A. J. van der Veen. Analytical method for blind binary signal separation. *IEEE Transactions on Signal Processing*, 45(4):1078–1082, April 1997.